PHYSICAL REVIEW D **80,** 074016 (2009)

Threshold resummation for dihadron production in hadronic collisions

Leandro G. Almeida[1] and George Sterman[1]
[1]*C. N. Yang Institute for Theoretical Physics, Stony Brook University, Stony Brook, New York 11794-3840, USA*

Werner Vogelsang[2]
[2]*Physics Department, Brookhaven National Laboratory, Upton, New York 11973, USA*
(Received 8 July 2009; published 19 October 2009)

We study the resummation of large logarithmic perturbative corrections to the partonic cross sections relevant for dihadron production in hadronic collisions, $H_1H_2 \to h_1h_2X$, at high invariant mass of the produced hadron pair. These corrections arise near the threshold for the partonic reaction and are associated with soft-gluon emission. We perform the resummation to next-to-leading logarithmic accuracy, and show how to incorporate consistently cuts in rapidity and transverse momentum of the observed particles. We present numerical results for fixed-target and ISR regimes and find enhancements over the next-to-leading order cross section, which significantly improve the agreement between theoretical predictions and data.

DOI: 10.1103/PhysRevD.80.074016 PACS numbers: 12.38.−t, 12.38.Bx, 12.38.Cy, 13.85.Ni

I. INTRODUCTION

Cross sections for hadron production in hadronic collisions play an important role in QCD. They offer a variety of insights into strong interaction dynamics. At sufficiently large momentum transfer in the reaction, QCD perturbation theory can be used to derive predictions. The cross section may be factorized at leading power in the hard scale into convolutions of long-distance factors representing the structure of the initial hadrons and the fragmentation of the final-state partons into the observed hadrons, and parts that are short-distance and describe the hard interactions of the partons. If the parton distribution functions and fragmentation functions are known from other processes, especially deeply inelastic scattering and e^+e^- annihilation, hadron production in hadronic collisions directly tests the factorized perturbative-QCD approach and the relevance of higher orders in the perturbative expansion.

Much emphasis in both theory and experiment has been on single-inclusive hadron production, $H_1H_2 \to hX$ [1–8]. Here the large momentum transfer is provided by the high transverse momentum of the observed hadron. Of equal importance, albeit explored to a somewhat lesser extent, is dihadron production, $H_1H_2 \to h_1h_2X$, when the pair is produced with large invariant mass M. In many ways, one may think of this process as a generalization of the Drell-Yan process to a completely hadronic situation, with the Drell-Yan lepton pair replaced by the hadron pair. The process is therefore particularly interesting for studying QCD dynamics, as we shall also see throughout this paper. Experimental data for dihadron production as a function of pair mass are available from various fixed-target experiments [9–11], as well as from the ISR [12]. On the theory side, next-to-leading order (NLO) calculations for this process are available [13–15]. They have been confronted with the available data sets, and it was found that overall agreement could only be achieved when rather small renormalization and factorization scales were chosen. The NLO calculations in fact show very large scale dependence. If more natural scales are chosen, NLO theory significantly underpredicts the cross section data, as we shall also confirm below.

In this paper, we investigate the all-order resummation of large logarithmic corrections to the partonic cross sections. This is of considerable interest for the comparison between data and the NLO calculation just described. A related resummation for the single-inclusive hadron cross section [5] was found to lead to significant enhancements of the predicted cross section over NLO, in much better overall agreement with the available data in that case.

At partonic threshold, when the initial partons have just enough energy to produce two partons with high invariant pair mass (which subsequently fragment into the observed hadron pair), the phase space available for gluon bremsstrahlung vanishes, resulting in large logarithmic corrections. To be more specific, if we consider the cross section as a function of the partonic pair mass $\hat{m}$, the partonic threshold is reached when $\hat{s} = \hat{m}^2$, that is, $\hat{\tau} \equiv \hat{m}^2/\hat{s} = 1$, where $\sqrt{\hat{s}}$ is the partonic center-of-mass system (c.m.s.) energy. The leading large contributions near threshold arise as $\alpha_s^k[\ln^{2k-1}(1-\hat{\tau})/(1-\hat{\tau})]_+$ at the kth order in perturbation theory, where α_s is the strong coupling and the ''plus'' distribution will be defined below. Sufficiently close to threshold, the perturbative series will be useful only if such terms are taken into account to all orders in α_s, which is what is achieved by threshold resummation [16–19]. Here we extend threshold resummation further, to cross sections involving cuts on individual hadron p_T and the rapidity of the pair.

We note that this behavior near threshold is very familiar from that in the Drell-Yan process, if one thinks of $\hat{m}$ as the

invariant mass of the lepton pair. Hadron pair production is more complex in that gluon emission will occur not only from initial-state partons, but also from those in the final state. Furthermore, interference between soft emissions from the various external legs is sensitive to the color exchange in the hard scattering, which gives rise to a special additional contribution to the resummation formula, derived in [17,20,21].

The larger $\hat{\tau}$, the more dominant the threshold logarithms will be. Because of this and the rapid falloff of the parton distributions and fragmentation functions with momentum fraction, threshold effects tend to become more and more relevant as the *hadronic* scaling variable $\tau \equiv M^2/S$ goes to one. This means that the fixed-target regime is the place where threshold resummation is expected to be particularly relevant and useful. We will indeed confirm this in our study. Nonetheless, because of the convolution form of the partonic cross sections and the parton distributions and fragmentation functions (see below), the threshold regime $\hat{\tau} \to 1$ plays an important role also at higher (collider) energies. Here one may, however, also have to incorporate higher-order terms that are subleading at partonic threshold.

In Sec. II we provide the basic formulas for the dihadron cross section as a function of pair mass at fixed order in perturbation theory, and display the role of the threshold region. Section III presents details of the threshold resummation for the cross section. In Sec. IV we give phenomenological results, comparing the threshold resummed calculation to the available experimental data. Finally, we summarize our results in Sec. V. Appendices A and B provide details of the NLO corrections to the perturbative cross section near threshold.

II. PERTURBATIVE CROSS SECTION AND PARTONIC THRESHOLD

We are interested in the hadronic cross section for the production of two hadrons $h_{1,2}$,

$$H_1(P_1) + H_2(P_2) \to h_1(K_1) + h_2(K_2) + X, \tag{1}$$

with pair invariant mass

$$M^2 \equiv (K_1 + K_2)^2. \tag{2}$$

We will consider the cross section differential in the rapidities η_1, η_2 of the two produced hadrons, treated as massless, in the c.m.s. of the initial hadrons, or in their difference and average,

$$\Delta\eta = \frac{1}{2}(\eta_1 - \eta_2), \tag{3}$$

$$\bar{\eta} = \frac{1}{2}(\eta_1 + \eta_2). \tag{4}$$

We will later integrate over regions of rapidity corresponding to the relevant experimental coverage. For sufficiently large M^2, the cross section for the process can be written in the factorized form

$$M^4 \frac{d\sigma^{H_1H_2\to h_1h_2X}}{dM^2 d\Delta\eta d\bar{\eta}} = \sum_{abcd} \int_0^1 dx_a dx_b dz_c dz_d f_a^{H_1}(x_a, \mu_{Fi}) f_b^{H_2}(x_b, \mu_{Fi}) z_c D_c^{h_1}(z_c, \mu_{Ff}) z_d D_d^{h_2}(z_d, \mu_{Ff}) \times \frac{\hat{m}^4 d\hat{\sigma}^{ab\to cd}}{d\hat{m}^2 d\Delta\eta d\bar{\eta}}\left(\hat{\tau}, \Delta\eta, \hat{\eta}, \alpha_s(\mu_R), \frac{\mu_R}{\hat{m}}, \frac{\mu_{Fi}}{\hat{m}}, \frac{\mu_{Ff}}{\hat{m}}\right), \tag{5}$$

where $\hat{\eta}$ is the average rapidity in the partonic c.m.s., which is related to $\bar{\eta}$ by

$$\hat{\eta} = \bar{\eta} - \frac{1}{2}\ln\left(\frac{x_a}{x_b}\right). \tag{6}$$

The quantity $\Delta\eta$ is a difference of rapidities and hence boost invariant. It is important to note that the rapidities of the hadrons with lightlike momenta K_1 and K_2 are the same as those of their lightlike parent partons. The average and relative rapidities for the hadrons and their parent partons are also therefore the same, a feature that we will use below. Furthermore, in Eq. (5) the $f_{a,b}^{H_{1,2}}$ are the parton distribution functions for partons *a, b* in hadrons $H_{1,2}$ and $D_{c,d}^{h_{1,2}}$ the fragmentation functions for partons *c, d* fragmenting into the observed hadrons $h_{1,2}$. The distribution functions are evaluated at the initial-state and final-state factorization scales μ_{Fi} and μ_{Ff}, respectively. μ_R denotes the renormalization scale. The $d\hat{\sigma}^{ab\to cd}/d\hat{\tau}d\bar{\eta}d\Delta\eta$ are the partonic differential cross sections for the contributing partonic processes $ab \to cdX'$, where X' denotes some additional unobserved partonic final state. The partonic momenta are given in terms of the hadronic ones by $p_a = x_aP_1$, $p_b = x_bP_2$, $p_c = K_1/z_c$, $p_d = K_2/z_d$. We introduce a set of variables, some of which have been used in Eq. (5):

$$S = (P_1 + P_2)^2, \tag{7}$$

$$\tau \equiv \frac{M^2}{S}, \tag{8}$$

$$\hat{s} \equiv (x_aP_1 + x_bP_2)^2 = x_ax_bS, \tag{9}$$

$$\hat{m}^2 \equiv \left(\frac{K_1}{z_c} + \frac{K_2}{z_d}\right)^2 = \frac{M^2}{z_cz_d}, \tag{10}$$

$$\hat{\tau} \equiv \frac{\hat{m}^2}{\hat{s}} = \frac{M^2}{x_a x_b z_c z_d S} = \frac{\tau}{x_a x_b z_c z_d}. \tag{11}$$

At the level of partonic scattering in the factorized cross section, Eq. (5), the other relevant variables are the partonic c.m.s. energy $\sqrt{\hat{s}}$, and the invariant mass $\hat{m}$ of the pair of partons that fragment into the observed dihadron pair. We have written Eq. (5) in such a way that the final factor is a dimensionless function. Hence, it can be chosen to be a function of the dimensionless ratio $\hat{m}^2/\hat{s} = \hat{\tau}$ and the ratio of $\hat{m}$ to the factorization and renormalization scales, as well as the rapidities and the strong coupling. In the following, we will take all factorization scales to be equal to the renormalization scale for simplicity, that is, $\mu_R = \mu_{Fi} = \mu_{Ff} \equiv \mu$. We then write

$$\frac{\hat{m}^4 d\hat{\sigma}^{ab\to cd}}{d\hat{m}^2 d\Delta\eta d\bar{\eta}}\left(\hat{\tau}, \Delta\eta, \hat{\eta}, \alpha_s(\mu), \frac{\mu}{\hat{m}}\right) \equiv \omega_{ab\to cd}\left(\hat{\tau}, \Delta\eta, \hat{\eta}, \alpha_s(\mu), \frac{\mu}{\hat{m}}\right). \tag{12}$$

The variable $\hat{\tau}$ is of special interest for threshold resummation, because it is a measure of the phase space available for radiation at short distances. The limit $\hat{\tau} \to 1$ corresponds to the partonic threshold, where the partonic hard scattering uses all available energy to produce the pair. This is kinematically similar to the Drell-Yan process, if one thinks of the hadron pair replaced by a lepton pair. The presence of fragmentation of course complicates the analysis somewhat, because only a fraction $z_c z_d$ of $\hat{m}^2$ is used for the invariant mass of the observed hadron pair. In the following it will in fact be convenient to also use the variable

$$\tau' \equiv \frac{\hat{m}^2}{S} = \frac{M^2}{z_c z_d S}, \tag{13}$$

which is the ratio of the partonic $\hat{m}^2$ to the overall c.m.s. invariant S and hence may be viewed as the "τ variable" at the level of produced partons when fragmentation has not yet been taken into account. This variable is close in spirit to the variable $\tau = Q^2/S$ in Drell-Yan.

The partonic cross sections can be computed in QCD perturbation theory, where they are expanded as

$$\omega_{ab\to cd} = \left(\frac{\alpha_s}{\pi}\right)^2\left[\omega^{\mathrm{LO}}_{ab\to cd} + \frac{\alpha_s}{\pi}\omega^{\mathrm{NLO}}_{ab\to cd} + \cdots\right]. \tag{14}$$

Here we have separated the overall power of $\mathcal{O}(\alpha_s^2)$, which arises because the leading-order (LO) partonic hard-scattering processes are the ordinary $2 \to 2$ QCD scatterings. At LO, one has $\hat{\tau} = 1$, and also the two partons are produced back-to-back in the partonic c.m.s., so that $\hat{\eta} = 0$. One can therefore write the LO term as

$$\omega^{\mathrm{LO}}_{ab\to cd}(\hat{\tau}, \Delta\eta, \hat{\eta}) = \delta(1-\hat{\tau})\delta(\hat{\eta})\omega^{(0)}_{ab\to cd}(\Delta\eta), \tag{15}$$

where $\omega^{(0)}_{ab\to cd}$ is a function of $\Delta\eta$ only. The second delta function implies that $\bar{\eta} = \frac{1}{2}\ln(x_a/x_b)$. At next-to-leading order, or overall $\mathcal{O}(\alpha_s^3)$, one can have $\hat{\tau} \neq 1$ and $\hat{\eta} \neq 0$. Near partonic threshold, $\hat{\tau} \to 1$, however, the kinematics becomes "LO like." The average rapidity of the final-state partons, c and d (and therefore of the observed dihadrons) is determined by the ratio x_a/x_b, up to corrections that vanish when the energy available for soft radiation is squeezed to zero. As noted in Ref. [22], in this limit the delta function that fixes the partonic pair rapidity $\hat{\eta}$ becomes independent of soft radiation, and may be factored out of the phase space integral over the latter. This is true at all orders in perturbation theory. One has:

$$\begin{aligned}\omega_{ab\to cd}(\hat{\tau}, \Delta\eta, \hat{\eta}, \alpha_s(\mu), \mu/\hat{m}) &= \delta(\hat{\eta})\omega^{\mathrm{sing}}_{ab\to cd}(\hat{\tau}, \Delta\eta, \alpha_s(\mu), \mu/\hat{m}) \\ &\quad + \omega^{\mathrm{reg}}_{ab\to cd}(\hat{\tau}, \Delta\eta, \hat{\eta}, \alpha_s(\mu), \mu/\hat{m}),\end{aligned} \tag{16}$$

where all singular behavior near threshold is contained in the functions $\omega^{\mathrm{sing}}_{ab\to cd}$. Threshold resummation addresses this singular part to all orders in the strong coupling. All remaining contributions, which are subleading near threshold, are collected in the "regular" functions $\omega^{\mathrm{reg}}_{ab\to cd}$. Specifically, for the NLO corrections, one finds the following structure:

$$\begin{aligned}&\omega^{\mathrm{NLO}}_{ab\to cd}(\hat{\tau}, \Delta\eta, \hat{\eta}, \mu/\hat{m}) \\ &= \delta(\hat{\eta})\Bigg[\omega^{(1,0)}_{ab\to cd}(\Delta\eta, \mu/\hat{m})\delta(1-\hat{\tau}) + \omega^{(1,1)}_{ab\to cd}(\Delta\eta, \mu/\hat{m}) \\ &\quad \times\left(\frac{1}{1-\hat{\tau}}\right)_+ + \omega^{(1,2)}_{ab\to cd}(\Delta\eta)\left(\frac{\log(1-\hat{\tau})}{1-\hat{\tau}}\right)_+\Bigg] \\ &\quad + \omega^{\mathrm{reg,NLO}}_{ab\to cd}(\hat{\tau}, \Delta\eta, \hat{\eta}, \mu/\hat{m}),\end{aligned} \tag{17}$$

where the singular part near threshold is represented by the functions $\omega^{(1,0)}_{ab\to cd}$, $\omega^{(1,1)}_{ab\to cd}$, $\omega^{(1,2)}_{ab\to cd}$, which are again functions of only $\Delta\eta$, up to scale dependence. The plus-distributions are defined by

$$\int_{x_0}^1 f(x)(g(x))_+ dx \equiv \int_{x_0}^1 (f(x) - f(1))g(x)dx - f(1)\int_0^{x_0} g(x)dx. \tag{18}$$

Appendix A describes the derivation of the coefficients $\omega^{(1,0)}_{ab\to cd}$, $\omega^{(1,1)}_{ab\to cd}$, $\omega^{(1,2)}_{ab\to cd}$ explicitly from a calculation of the NLO corrections near threshold. This will serve as a useful check on the correctness of the resummed formula, and also to determine certain matching coefficients.

As suggested above, the structure given in Eq. (17) is similar to that found for the Drell-Yan cross section at NLO. A difference is that in the inclusive Drell-Yan case one can integrate over all $\Delta\eta$ to obtain a total cross section. This integration is finite because the LO process in Drell-Yan is the s-channel reaction $q\bar{q} \to \ell^+\ell^-$. In the case of dihadrons, the LO QCD processes also have t as well as

u-channel contributions, which cause the integral over $\Delta\eta$ to diverge when the two hadrons are produced back-to-back with large mass, but each parallel or antiparallel to the initial beams. As a result, one will always need to consider only a finite range in $\Delta\eta$. This is, of course, not a problem as this is anyway also done in experiment. It does, however, require a slightly more elaborate analysis for threshold resummation, which we review below.

III. THRESHOLD RESUMMATION FOR DIHADRON PAIRS

A. Hard scales and transforms

The resummation of the logarithmic corrections is organized in Mellin-N moment space [16]. In moment space, the partonic cross sections absorb logarithmic corrections associated with the emission of soft and collinear gluons to all orders. Employing appropriate moments, which we will identify shortly, we will see that the convolutions among the different nonperturbative and perturbative regions in the hadronic cross section decouple.

In terms of the dimensionless hard-scattering function introduced in Eq. (12) the hadronic cross section in Eq. (5) becomes

$$M^4\frac{d\sigma^{H_1H_2\to h_1h_2X}}{dM^2d\Delta\eta d\bar{\eta}}=\sum_{abcd}\int_0^1 dx_a dx_b dz_c dz_d f_a^{H_1}(x_a)f_b^{H_2}(x_b)\times z_c D_c^{h_1}(z_c) z_d D_d^{h_2}(z_d)\times\omega_{ab\to cd}\left(\hat{\tau},\Delta\eta,\hat{\eta},\alpha_s(\mu),\frac{\mu}{\hat{m}}\right), \quad (19)$$

where for simplicity we have dropped the scale dependence of the parton distributions and fragmentation functions. At lowest order, when the hard-scattering function $\omega_{ab\to cd}$ is given by Eq. (15), the cross section is found to factorize under ''double'' moments [23,24], a Mellin moment with respect to $\tau=M^2/S$ and a Fourier moment in $\bar{\eta}=\hat{\eta}+\frac{1}{2}\ln(x_a/x_b)$:

$$\int_{-\infty}^{\infty}d\bar{\eta}e^{i\nu\bar{\eta}}\int_0^1 d\tau\tau^{N-1}M^4\frac{d\sigma^{H_1H_2\to h_1h_2X}}{dM^2d\Delta\eta d\bar{\eta}}\bigg|_{\rm LO}=\sum_{abcd}\tilde{f}_a^{H_1}(N+1+i\nu/2)\tilde{f}_b^{H_2}(N+1-i\nu/2)\times\tilde{D}_c^{h_1}(N+2)\tilde{D}_d^{h_2}(N+2)\int_{-\infty}^{\infty}d\hat{\eta}e^{i\nu\hat{\eta}}\times\int_0^1 d\hat{\tau}\hat{\tau}^{N-1}\delta(1-\hat{\tau})\delta(\hat{\eta})\left(\frac{\alpha_s(\mu)}{\pi}\right)^2\omega_{ab\to cd}^{(0)}(\Delta\eta), \quad (20)$$

where the Mellin moments of the parton distributions or fragmentation functions are defined in the usual way, for example

$$\tilde{f}_a^H(N)\equiv\int_0^1 x^{N-1}f_a^H(x)dx. \quad (21)$$

We note that instead of a combined Mellin and Fourier transform one may equivalently use a suitable double-Mellin transform [25]. The last two integrals in Eq. (20) give the combined Mellin and Fourier moment of the LO partonic cross section. Because of the two delta functions, they are trivial and just yield the N and ν independent result $(\alpha_s/\pi)^2\omega_{ab\to cd}^{(0)}(\Delta\eta)$. One might expect that this generalizes to higher orders, so that the double moments

$$\int_{-\infty}^{\infty}d\hat{\eta}e^{i\nu\hat{\eta}}\int_0^1 d\hat{\tau}\hat{\tau}^{N-1}\omega_{ab\to cd}\left(\hat{\tau},\Delta\eta,\hat{\eta},\alpha_s(\mu),\frac{\mu}{\hat{m}}\right) \quad (22)$$

would appear times moments of fragmentation functions. However, this is impeded by the presence of the renormalization/factorization scale μ which must necessarily enter in a ratio with $\hat{m}=M/\sqrt{z_c z_d}$. As a result of this dependence on z_c and z_d, the moments $\tilde{D}_c^{h_1}(N+2)$, $\tilde{D}_d^{h_2}(N+2)$ of the fragmentation functions will no longer be generated, and the factorized cross section does not separate into a product under moments. Physically, this is a reflection of the mismatch between the *observed* scale, the dihadron mass M, and the *unobserved* threshold scale at the hard scattering, $\hat{m}$. Threshold logarithms appear when $\hat{s}$ approaches the latter scale, not the former. This implies that at fixed M there is actually a range of hard-scattering partonic thresholds, extending all the way from M at the lower end to $\sqrt{S}$ at the upper. This situation is to be contrasted to the Drell-Yan process or to dijet production at fixed masses, where the underlying hard scale is defined directly by the observable.

We will deal with the presence of this range of hard scales $\hat{m}$ by carrying out threshold resummation at fixed $\hat{m}$ as well as at fixed factorization/renormalization scale. For this purpose, we rewrite the cross section (19) in a form that isolates the fragmentation functions:

$$M^4\frac{d\sigma^{H_1H_2\to h_1h_2X}}{dM^2d\Delta\eta d\bar{\eta}}=\sum_{cd}\int_0^1 dz_c dz_d z_c D_c^{h_1}(z_c,\mu)\times z_d D_d^{h_2}(z_d,\mu)\times\Omega_{H_1H_2\to cd}\left(\tau',\Delta\eta,\bar{\eta},\alpha_s(\mu),\frac{\mu}{\hat{m}}\right), \quad (23)$$

where again $\tau'=\hat{m}^2/S=\hat{\tau}x_a x_b$ and $\Omega_{H_1H_2\to cd}$ is given by the convolution of the parton distribution functions and $\omega_{ab\to cd}$:

$$\Omega_{H_1H_2\to cd}\left(\tau',\Delta\eta,\bar{\eta},\alpha_s(\mu),\frac{\mu}{\hat{m}}\right)=\sum_{ab}\int_0^1 dx_a dx_b f_a^{H_1}(x_a,\mu)f_b^{H_2}(x_b,\mu)\times\omega_{ab\to cd}\left(\hat{\tau},\Delta\eta,\hat{\eta},\alpha_s(\mu),\frac{\mu}{\hat{m}}\right), \quad (24)$$

with $\hat{\eta} = \bar{\eta} - \frac{1}{2}\ln(x_a/x_b)$ as before. At fixed final-state *partonic* mass $\hat{m}$, the function $\Omega_{H_1H_2\to cd}$ now has the desired factorization property under Fourier and Mellin transforms:

$$\int_{-\infty}^{\infty} d\bar{\eta} e^{i\nu\bar{\eta}} \int_0^1 d\tau' (\tau')^{N-1} \Omega_{H_1H_2\to cd}\left(\tau', \Delta\eta, \bar{\eta}, \alpha_s(\mu), \frac{\mu}{\hat{m}}\right) = \sum_{ab} \tilde{f}_a^{H_1}(N+1+i\nu/2, \mu) \tilde{f}_b^{H_2}(N+1-i\nu/2, \mu) \times \tilde{\omega}_{ab\to cd}\left(N, \nu, \Delta\eta, \alpha_s(\mu), \frac{\mu}{\hat{m}}\right), \tag{25}$$

where

$$\tilde{\omega}_{ab\to cd}\left(N, \nu, \Delta\eta, \alpha_s(\mu), \frac{\mu}{\hat{m}}\right) \equiv \int_{-\infty}^{\infty} d\hat{\eta} e^{i\nu\hat{\eta}} \int_0^1 d\hat{\tau} \hat{\tau}^{N-1} \omega_{ab\to cd}\left(\hat{\tau}, \Delta\eta, \hat{\eta}, \alpha_s(\mu), \frac{\mu}{\hat{m}}\right). \tag{26}$$

Through Eqs. (23)–(26) we have formulated the hadronic cross section in a way that involves moment-space expressions for the partonic hard-scattering functions, which may be resummed. Because the final-state fractions z_i equal unity at partonic threshold, the scale $\hat{m}$ in the short-distance function may be identified here with the final-state partonic invariant mass, up to corrections that are suppressed by powers of N. For the singular, resummed short-distance function we therefore do not encounter the problem with the moments discussed above in connection with Eq. (22).

B. Resummation at next-to-leading logarithm (NLL)

As we saw in Eq. (16), the singular parts of the partonic cross sections near threshold enter with $\delta(\hat{\eta})$. This gives for the corresponding moment-space expression

$$\tilde{\omega}^{\text{resum}}_{ab\to cd}\left(N, \Delta\eta, \alpha_s(\mu), \frac{\mu}{\hat{m}}\right) = \int_0^1 d\hat{\tau} \hat{\tau}^{N-1} \omega^{\text{sing}}_{ab\to cd}\left(\hat{\tau}, \Delta\eta, \alpha_s(\mu), \frac{\mu}{\hat{m}}\right), \tag{27}$$

which is a function of N only, but not of the Fourier variable ν. Dependence on the Fourier variable ν then resides entirely in the parton distributions. It is this function, $\tilde{\omega}^{\text{resum}}_{ab\to cd}$, that threshold resummation addresses, which is the reason for the use of the label "resum" from now on.

The nature of singularities at partonic threshold is determined by the available phase space for radiation as $\hat{\tau} \to 1$. Denoting by k^μ the combined momentum of all radiation, whether from the incoming partons a and b or the outgoing partons c and d, one has

$$1 - \hat{\tau} = 1 - \frac{(p_c + p_d)^2}{(p_a + p_b)^2} = 1 - \frac{(p_a + p_b - k)^2}{(p_a + p_b)^2} \approx \frac{2k_0^*}{\sqrt{\hat{s}}}, \tag{28}$$

where k_0^* is the energy of the soft radiation in the c.m.s of the initial partons.

At partonic threshold, the cross section factorizes into "jet" functions associated with the two incoming and outgoing partons, in addition to an overall soft matrix, traced against the color matrix describing the hard scattering [17,20]. Corrections to this factorized structure are suppressed by powers of $1 - \hat{\tau}$. The total cross section is a convolution in energy between these functions, which is factorized into a product by moments in $\hat{\tau}^N \sim \exp[-N(1-\hat{\tau})]$, again with corrections suppressed by powers of $(1 - \hat{\tau})$, or equivalently, powers of N. This result was demonstrated for jet cross sections in [20], and the extension to observed hadrons in the final state was discussed in [26,27]. The resummed expression for the partonic hard-scattering function for the process $ab \to cd$ then reads [17,18,20,21]:

$$\tilde{\omega}^{\text{resum}}_{ab\to cd}\left(N, \Delta\eta, \alpha_s(\mu), \frac{\mu}{\hat{m}}\right) = \Delta_a^{N+1}\left(\alpha_s(\mu), \frac{\mu}{\hat{m}}\right) \Delta_b^{N+1}\left(\alpha_s(\mu), \frac{\mu}{\hat{m}}\right) \times \text{Tr}\{H \mathcal{S}_N^\dagger S \mathcal{S}_N\}_{ab\to cd}\left(\Delta\eta, \alpha_s(\mu), \frac{\mu}{\hat{m}}\right) \times \Delta_c^{N+2}\left(\alpha_s(\mu), \frac{\mu}{\hat{m}}\right) \Delta_d^{N+2}\left(\alpha_s(\mu), \frac{\mu}{\hat{m}}\right). \tag{29}$$

We will now discuss each of the functions and give their expansions to next-to-leading logarithmic (NLL) accuracy.

The Δ_i^N $(i = a, b, c, d)$ represent the effects of soft-gluon radiation collinear to an initial or final parton. Working in the $\overline{\text{MS}}$ scheme, one has [16–18,20,21]:

$$\ln\Delta_i^N\left(\alpha_s(\mu), \frac{\mu}{\hat{m}}\right) = \int_0^1 \frac{z^{N-1} - 1}{1 - z} \int_{\hat{m}^2}^{(1-z)^2\hat{m}^2} \frac{dq^2}{q^2} A_i(\alpha_s(q^2)) + \int_{\mu^2}^{\hat{m}^2} \frac{dq^2}{q^2}\left[-A_i(\alpha_s(q^2)) \ln\bar{N} - \frac{1}{2} B_i(\alpha_s(q^2))\right]. \tag{30}$$

Here the functions A_i and B_i are perturbative series in α_s,

$$A_i(\alpha_s) = \frac{\alpha_s}{\pi} A_i^{(1)} + \left(\frac{\alpha_s}{\pi}\right)^2 A_i^{(2)} + \cdots, \tag{31}$$

and likewise for B_i. To NLL, one needs the coefficients [28]:

$$A_i^{(1)} = C_i, \qquad A_a^{(2)} = \frac{1}{2} C_i\left[C_A\left(\frac{67}{18} - \frac{\pi^2}{6}\right) - \frac{5}{9} N_f\right], \qquad B_q^{(1)} = -\frac{3}{2} C_F, \qquad B_g^{(1)} = -2\pi b_0, \tag{32}$$

where N_f is the number of flavors, and

$$C_q = C_F = \frac{N_c^2 - 1}{2N_c} = \frac{4}{3}, \qquad C_g = C_A = N_c = 3,$$
$$b_0 = \frac{11C_A - 2N_f}{12\pi}. \tag{33}$$

The factors Δ_i^N generate leading threshold enhancements, due to soft-collinear radiation. We note that our expression for the Δ_i^N differs by the N-independent term proportional to $B_i^{(1)}$ from that often used in studies of threshold resummation (see, for example, Refs. [18,29]). As was shown in [17,20,21], this term is part of the resummed expression and exponentiates. In fact, the second term on the right-hand side of Eq. (30) contains the large-N part of the moments of the diagonal quark and gluon splitting functions, matching the full leading power μ_F-dependence of the parton distributions and fragmentation functions in Eqs. (23) and (25). We shall return to this point below.

Each of the functions $H_{ab\to cd}$, $\mathcal{S}_{N,ab\to cd}$, $S_{ab\to cd}$ in Eq. (29) is a matrix in a space of color exchange operators [17,20], and the trace is taken in this space. Note that this part is the only one in the resummed expression Eq. (29) that carries dependence on $\Delta\eta$. The $H_{ab\to cd}$ are the hard-scattering functions. They are perturbative and have the expansion

$$H_{ab\to cd}\left(\Delta\eta, \alpha_s(\mu), \frac{\mu}{\hat{m}}\right) = H^{(0)}_{ab\to cd}(\Delta\eta) + \frac{\alpha_s(\mu)}{\pi} H^{(1)}_{ab\to cd}\left(\Delta\eta, \frac{\mu}{\hat{m}}\right) + \mathcal{O}(\alpha_s^2). \tag{34}$$

The LO (i.e. $\mathcal{O}(\alpha_s^2)$) parts $H^{(0)}_{ab\to cd}$ are known [17,20,21], but the first-order corrections have not been derived yet. We shall return to this point shortly. The $S_{ab\to cd}$ are soft functions. They depend on N only through the argument of the running coupling, which is set to μ/N [17], and have the expansion

$$S_{ab\to cd}\left(\Delta\eta, \alpha_s, \frac{\mu}{\hat{m}}\right) = S^{(0)}_{ab\to cd} + \frac{\alpha_s}{\pi} S^{(1)}_{ab\to cd}\left(\Delta\eta, \frac{\mu}{N\hat{m}}\right) + \mathcal{O}(\alpha_s^2). \tag{35}$$

The N-dependence of the soft function enters the resummed cross section at the level of next-to-next-to-leading logarithms. The LO terms $S^{(0)}_{ab\to cd}$ may also be found in [17,20,21]. They are independent of $\Delta\eta$.

The resummation of wide-angle soft gluons is contained in the $\mathcal{S}_{ab\to cd}$, which are exponentials and given in terms of soft anomalous dimensions, $\Gamma_{ab\to cd}$:

$$\mathcal{S}_{N,ab\to cd}\left(\Delta\eta, \alpha_s(\mu), \frac{\mu}{\hat{m}}\right) = \mathcal{P}\exp\left[\frac{1}{2}\int_{\hat{m}^2}^{\hat{m}^2/\bar{N}^2} \frac{dq^2}{q^2}\Gamma_{ab\to cd}(\Delta\eta, \alpha_s(q^2))\right], \tag{36}$$

where $\mathcal{P}$ denotes path ordering and where $\bar{N} \equiv Ne^{\gamma_E}$ with γ_E is the Euler constant. The soft anomalous dimension matrices start at $\mathcal{O}(\alpha_s)$,

$$\Gamma_{ab\to cd}(\Delta\eta, \alpha_s) = \frac{\alpha_s}{\pi}\Gamma^{(1)}_{ab\to cd}(\Delta\eta) + \mathcal{O}(\alpha_s^2). \tag{37}$$

Their first-order terms are presented in [17,20,21,30].

Note that the Born cross sections are recovered by computing $\mathrm{Tr}\{H^{(0)}S^{(0)}\}_{ab\to cd}$, which is proportional to the function $\omega^{(0)}_{ab\to cd}(\Delta\eta)$ introduced in Eq. (15). It is instructive to consider the expansion of the trace part in Eq. (29) to first order in α_s. One finds [31]:

$$\mathrm{Tr}\{H\mathcal{S}_N^\dagger S\mathcal{S}_N\}_{ab\to cd} = \mathrm{Tr}\{H^{(0)}S^{(0)}\}_{ab\to cd} + \frac{\alpha_s}{\pi}\mathrm{Tr}\{-[H^{(0)}(\Gamma^{(1)})^\dagger S^{(0)} + H^{(0)}S^{(0)}\Gamma^{(1)}]\ln\bar{N} + H^{(1)}S^{(0)} + H^{(0)}S^{(1)}\}_{ab\to cd} + \mathcal{O}(\alpha_s^2). \tag{38}$$

When combined with the first-order expansion of the factors Δ_i^N in Eq. (29), one obtains

$$\tilde{\omega}^{\mathrm{resum}}_{ab\to cd}\left(N, \Delta\eta, \alpha_s(\mu), \frac{\mu}{\hat{m}}\right) = \mathrm{Tr}\{H^{(0)}S^{(0)}\}_{ab\to cd}\left(1 + \frac{\alpha_s}{\pi}\sum_{i=a,b,c,d} A_i^{(1)}[\ln^2\bar{N} + \ln\bar{N}\ln(\mu^2/\hat{m}^2)]\right) + \frac{\alpha_s}{\pi}\mathrm{Tr}\{-[H^{(0)}(\Gamma^{(1)})^\dagger S^{(0)} + H^{(0)}S^{(0)}\Gamma^{(1)}]\ln\bar{N} + H^{(1)}S^{(0)} + H^{(0)}S^{(1)}\}_{ab\to cd} + \mathcal{O}(\alpha_s^2). \tag{39}$$

This expression can be compared to the results of the explicit NLO calculation near threshold given in Appendix A. This provides a cross-check on the terms that are logarithmic in N, that is, singular at threshold. From comparison to the part proportional to $\delta(1-\hat{\tau})$ in the NLO expression, one will be able to read off the combination $(H^{(1)}S^{(0)} + H^{(0)}S^{(1)})$ in Eq. (39). This is, of course, not sufficient to determine the full first-order matrices $H^{(1)}$ and $S^{(1)}$, which would be needed to fully evaluate the trace part in Eq. (29) to NLL. To derive $H^{(1)}$ and $S^{(1)}$, one would need to perform the NLO calculation near threshold in terms of a color decomposition [32], which is beyond the scope of this work. Instead, we use here an approximation that has been made in previous studies (see, for example, Ref. [5]),

$$\mathrm{Tr}\{H\mathcal{S}_N^\dagger S\mathcal{S}_N\}_{ab\to cd} \approx \left(1 + \frac{\alpha_s}{\pi}C^{(1)}_{ab\to cd}\right) \times \mathrm{Tr}\{H^{(0)}\mathcal{S}_N^\dagger S^{(0)}\mathcal{S}_N\}_{ab\to cd}, \tag{40}$$

where

$$C^{(1)}_{ab\to cd}(\Delta\eta, \mu/\hat{m}) \equiv \frac{\mathrm{Tr}\{H^{(1)}S^{(0)} + H^{(0)}S^{(1)}\}_{ab\to cd}}{\mathrm{Tr}\{H^{(0)}S^{(0)}\}_{ab\to cd}} \quad (41)$$

are referred to as "C coefficients." The coefficients we obtain for the various partonic channels are given in Appendix B. The approximation we have made becomes exact if only one color configuration contributes or if all eigenvalues of the soft anomalous dimension matrix are equal. By construction, it is also correct to first order in α_s.

We now turn to the explicit NLL expansions of the ingredients in the resummed partonic cross section. For the function Δ_i^N in Eq. (30) one finds:

$$\ln\Delta_i^N\left(\alpha_s(\mu), \frac{\mu}{\hat{m}}\right) = h_i^{(1)}(\lambda)\ln\bar{N} + h_i^{(2)}\left(\lambda, \alpha_s(\mu), \frac{\mu}{\hat{m}}\right) + \ln\mathcal{E}_i\left(\lambda, \alpha_s(\mu), \frac{\mu}{\hat{m}}\right), \quad (42)$$

where $\lambda = b_0\alpha_s(\mu)\ln\bar{N}$ and the functions $h_i^{(1)}$, $h_i^{(2)}$, $\ln(\mathcal{E}_i)$ are given by

$$\begin{aligned}
h_i^{(1)}(\lambda) &= \frac{A_i^{(1)}}{2\pi b_0\lambda}(2\lambda + \ln(1-2\lambda)),\\
h_i^{(2)}\left(\lambda, \alpha_s(\mu), \frac{\mu}{\hat{m}}\right) &= \frac{2\lambda + \ln(1-2\lambda)}{2\pi b_0}\left(\frac{A_i^{(1)}b_1}{b_0^2} - \frac{A_i^{(2)}}{\pi b_0} - A_i^{(1)}\ln\frac{\mu^2}{\hat{m}^2}\right) + \frac{A_i^{(1)}b_1}{4\pi b_0^3}\ln^2(1-2\lambda) + \frac{B_i^{(1)}}{2\pi b_0}\ln(1-2\lambda),\\
\ln\mathcal{E}_i\left(\lambda, \alpha_s(\mu), \frac{\mu}{\hat{m}}\right) &= \frac{1}{\pi b_0}\left(-A_i^{(1)}\ln\bar{N} - \frac{1}{2}B_i^{(1)}\right)\left[\ln(1-2\lambda) - b_0\alpha_s(\mu)\ln\frac{\mu^2}{\hat{m}^2}\right].
\end{aligned} \quad (43)$$

We note that we have written Eq. (42) in a "nonstandard" form that is actually somewhat more complex than necessary. For example, one can immediately see that the terms proportional to $B_i^{(1)}\ln(1-2\lambda)$ cancel between the functions $h_i^{(2)}$ and $\ln(\mathcal{E}_i)$, as they must because they were not present in the Δ_i^N in Eq. (30) in the first place. The term proportional to $\ln(\mu^2/\hat{m}^2)$ in $\ln(\mathcal{E}_i)$ is the expansion of the second term in Eq. (30). Its contribution involving $B_i^{(1)}$ does not carry logarithmic dependence on N and would normally be part of the C coefficients discussed above. The term proportional to $\ln(1-2\lambda)$ in $\ln(\mathcal{E}_i)$ has been separated from the first term in Eq. (30). Our motivation to use this form of Eq. (42) is that the piece termed $\ln(\mathcal{E}_i)$ may be viewed as resulting from a large-N leading-order evolution of the corresponding parton distribution or fragmentation function between scales $\hat{m}/\bar{N}$ and the factorization scale μ_F (we remind the reader that we have set the factorization and renormalization scales equal and denoted them by μ). As mentioned earlier, the factors $(-2A_i^{(1)}\ln\bar{N} - B_i^{(1)})$ correspond to the moments of the flavor-diagonal splitting functions, P_{ii}^N, while the term in square brackets is a LO approximation to

$$b_0\int_{\mu_F}^{\hat{m}^2/\bar{N}^2}\frac{dq^2}{q^2}\alpha_s(q^2). \quad (44)$$

Therefore, it is natural to identify [33]

$$\mathcal{E}_i\left(\lambda, \alpha_s(\mu), \frac{\mu}{\hat{m}}\right)\tilde{f}_i^H(N,\mu) \leftrightarrow \tilde{f}_i^H(N, \hat{m}/\bar{N}), \quad (45)$$

that is, the exponential related to $\mathcal{E}_i$ evolves the parton distributions from the factorization scale to the scale $\hat{m}/\bar{N}$, and likewise for the fragmentation functions. At the level of diagonal evolution, it makes of course no difference if $\ln(\mathcal{E}_i)$ is used to evolve the parton distributions or if it is just added to the function $h_i^{(2)}$. However, as was discussed in [33,34], one can actually promote the diagonal evolution expressed by $\mathcal{E}_i$ to the full singlet case by replacing the term $(-2A_i^{(1)}\ln\bar{N} - B_i^{(1)})$ by the full matrix of the moments of the LO singlet splitting functions, $P_{ij}^{(1),N}$, so that $\mathcal{E}$ itself becomes a matrix. Using this matrix in Eq. (42) instead of the diagonal $\mathcal{E}_i$, one takes into account terms that are suppressed as $1/N$ or higher. In particular, one resums terms of the form $\alpha_s^k\ln^{2k-1}\bar{N}/N$ to all orders in α_s [34]. We will mostly stick to the ordinary resummation based on a diagonal evolution operator $\mathcal{E}_i$ in this paper. However, as we shall show later in one example, the subleading terms taken into account by implementing the nondiagonal evolution in the parton distributions and fragmentation functions can actually be quite relevant in kinematic regimes where one is further away from threshold. Here we will only take the LO part of evolution into account, extension to NLO is possible and has been discussed in [33].

For a complete NLL resummation one also needs the expansion of the integral in Eq. (36), which leads to

$$\ln\mathcal{S}_{N,ab\to cd}\left(\Delta\eta, \alpha_s(\mu), \frac{\mu}{\hat{m}}\right) = \frac{\ln(1-2\lambda)}{2\pi b_0}\Gamma^{(1)}_{ab\to cd}(\Delta\eta). \quad (46)$$

As in [29], we perform the exponentiation of the matrix on the right-hand side numerically, by iterating the exponential series to an adequately large order.

C. Inverse of the Mellin and Fourier transform and matching procedure

As we have discussed in detail, the resummation is achieved in Mellin moment space. In order to obtain a resummed cross section in τ space, one needs an inverse

Mellin transform, accompanied by an inverse Fourier transform that reconstructs the dependence on $\bar{\eta}$. The Mellin inverse requires a prescription for dealing with the singularity in the perturbative strong coupling constant in Eqs. (30) and (36) or in the NLL expansions, Eqs. (42) and (43). We will use the *minimal prescription* developed in Ref. [35], which relies on use of the NLL expanded forms Eqs. (42) and (43), and on choosing a Mellin contour in complex-N space that lies to the *left* of the poles at $\lambda = 1/2$ and $\lambda = 1$ in the Mellin integrand. From Eqs. (25) and (26), we find

$$\Omega^{\rm resum}_{H_1H_2\to cd}\left(\tau', \Delta\eta, \bar{\eta}, \alpha_s(\mu), \frac{\mu}{\hat{m}}\right) = \frac{1}{2\pi}\int_{-\infty}^{\infty} d\nu e^{-i\nu\bar{\eta}} \int_{C_{\rm MP}-i\infty}^{C_{\rm MP}+i\infty} \frac{dN}{2\pi i}(\tau')^{-N} \times \sum_{ab} \tilde{f}_a^{H_1}(N+1+i\nu/2, \mu)\tilde{f}_b^{H_2}(N+1-i\nu/2, \mu) \times \tilde{\omega}^{\rm resum}_{ab\to cd}\left(N, \nu, \Delta\eta, \alpha_s(\mu), \frac{\mu}{\hat{m}}\right), \quad (47)$$

where the Mellin contour is chosen so that $b_0\alpha_s(\mu_R^2)\times \ln C_{\rm MP} < 1/2$, but all other poles in the integrand are as usual to the left of the contour. The result defined by the minimal prescription has the property that its perturbative expansion is an asymptotic series that has no factorial divergence and therefore no ''built-in'' powerlike ambiguities [35]. Power corrections may then be added as phenomenologically required. For most of our discussion below, the resummed short-distance function $\tilde{\omega}^{\rm resum}_{ab\to cd}$ is specified directly by Eqs. (42) and (43). When we refer to ''full singlet evolution,'' however, we make the identification in Eq. (45), and evolve the parton distributions and fragmentation functions to scale $\hat{m}/\bar{N}$. In this case the exponential in $\tilde{\omega}^{\rm resum}_{ab\to cd}$ is found from the $h_i^{(1)}$ and $h_i^{(2)}$ terms only in Eq. (42).

We note that the parton distribution functions in moment space fall off with an inverse power of the Mellin moment, typically as $1/N^4$ or faster. This helps very significantly to make the inverse Mellin integral in Eq. (47) numerically stable. In particular, the resulting functions $\Omega^{\rm resum}_{H_1H_2\to cd}$ are very well behaved at high τ'. This would be very different if one were to invert just the resummed partonic cross sections $\tilde{\omega}^{\rm resum}_{ab\to cd}$ and attempt to convolute the result with the parton distributions. The good behavior of the $\Omega^{\rm resum}_{H_1H_2\to cd}$ makes it straightforward numerically to insert them into Eq. (23), where they are convoluted with the fragmentation functions in terms of momentum fractions z at fixed rapidities. At this stage, it is straightforward to impose cuts in the transverse momenta and rapidities of the observed particles. This gives the final hadronic cross section $M^4 d\sigma^{H_1H_2\to h_1h_2X}/dM^2 d\Delta\eta d\bar{\eta}$. We note that because of the presence of the Landau pole and the definition of the Mellin contour in the minimal prescription, the inverted $\Omega^{\rm resum}_{H_1H_2\to cd}$ has support at $\tau' > 1$, where it is however decreasing exponentially with τ'. The numerical contribution from this region is very small (less than 1%) for all of the kinematics relevant for phenomenology.

When performing the resummation, one of course wants to make full use of the available fixed-order cross section, which in our case is NLO [$\mathcal{O}(\alpha_s^3)$]. Therefore, a matching to this cross section is appropriate, which may be achieved by expanding the resummed cross section to $\mathcal{O}(\alpha_s^3)$, subtracting the expanded result from the resummed one, and adding the full NLO cross section. Schematically:

$$d\sigma^{\rm match} = (d\sigma^{\rm resum} - d\sigma^{\rm resum}|_{\mathcal{O}(\alpha_s^3)}) + d\sigma^{\rm NLO}. \quad (48)$$

In this way, NLO is taken into account in full, and the soft-gluon contributions beyond NLO are resummed to NLL. Any double counting of perturbative orders is avoided.

IV. PHENOMENOLOGICAL RESULTS

We now compare our resummed calculations to experimental dihadron production data given as functions of the pair mass, M. These are available from the fixed-target experiments NA24 [9] (pp scattering at beam energy $E_p = 300$ GeV), E711 [10] (protons with $E_p = 800$ GeV on beryllium), and E706 [11] (pp and pBe with $E_p = 500$ and 800 GeV), as well as from the ISR pp collider experiment CCOR [12] which produced data at $\sqrt{S} = 44.8$ and 62.4 GeV. The data sets refer to a $\pi^0\pi^0 X$ final state, with the exception of E711, which measured the final states h^+h^+X, h^-h^-X, h^+h^-X with h summed over all possible hadron species. When presenting our results for this data set, we will follow [14] to consider for simplicity only the *summed* charged-hadron combination $(h^+ + h^-)\times(h^+ + h^-)X$. For this combination also the information on the fragmentation functions is more reliable than for individual charge states.

In each of the experimental data sets, kinematic cuts have been applied. These are variously on the individual hadron transverse momenta $p_{T,i}$ or rapidities η_i, or on variables that are defined from both hadrons, $\cos\theta^*$, Y, $p_T^{\rm pair}$. Here $\cos\theta^*$ is the mean of the cosines of the angles between the observed hadron directions and the closest beam directions, in a frame where the produced hadrons have equal and opposite longitudinal momenta, $p_{T,1}\sinh\eta_1 = -p_{T,2}\sinh\eta_2$ [9–12,14]. This system approximately coincides with the partonic c.m.s. In terms of the observed transverse momenta and rapidity difference one has:

$$\cos\theta^* = \frac{1}{2}\left(\frac{p_{T,1}}{p_{T,2} + p_{T,1}\cosh(2\Delta\eta)} + \frac{p_{T,2}}{p_{T,1} + p_{T,2}\cosh(2\Delta\eta)}\right)\sinh(2\Delta\eta). \quad (49)$$

Furthermore, Y is the rapidity of the pion pair,

$$Y = \frac{1}{2}\ln\left(\frac{\kappa^0 + \kappa^3}{\kappa^0 - \kappa^3}\right) = \bar{\eta} - \frac{1}{2}\ln\left(\frac{p_{T,1}e^{-\Delta\eta} + p_{T,2}e^{\Delta\eta}}{p_{T,1}e^{\Delta\eta} + p_{T,2}e^{-\Delta\eta}}\right), \tag{50}$$

where $\kappa = K_1 + K_2$ is the pair's four-momentum and where the second equality in terms of $\Delta\eta$, $\bar{\eta}$ and the hadron transverse momenta $p_{T,i}$ holds for LO kinematics as appropriate in the threshold regime. Finally, p_T^{pair} is the transverse momentum of the pion pair,

$$p_T^{\text{pair}} = |\mathbf{p}_{T,1} + \mathbf{p}_{T,2}| = |p_{T,1} - p_{T,2}|, \tag{51}$$

where again the second equality holds to LO. Thanks to our way of organizing the threshold resummed cross section, inclusion of cuts on any of these variables is straightforward.

In all our calculations, we use the CTEQ6M5 set of parton distribution functions [36], along with its associated value of the strong coupling constant. We furthermore for the most part use the "de Florian-Sassot-Stratmann" (DSS) fragmentation functions [37], but will also include comparisons to the results obtained for the most recent "Albino-Kniehl-Kramer" (AKK) set [38]. We note that one might argue that the use of NLO parton distribution functions and fragmentation functions is not completely justified for obtaining resummed predictions, given that large-N resummation effects are typically not included in their extraction mostly from deeply inelastic scattering (DIS) and e^+e^- annihilation data, respectively. As was shown in Ref. [39] for the case of the Drell-Yan process, resummation effects in the parton distribution functions extracted from DIS appear to have a very modest impact, except when high momentum fractions and/or relatively low scales are probed, which is not the case for the data sets we are considering here. We expect the same to hold for the fragmentation functions. In fact, some large-N resummation effects have been included in the AKK analysis [38], and comparisons to the results obtained for this set will therefore be interesting.

We choose for our calculations the renormalization and factorization scales to be equal, and we give them the values M and $2M$, in order to investigate the scale dependence of the results. One expects that a natural scale choice would be offered by the hard scale in the partonic scattering, which is $\mathcal{O}(\hat{m})$. Because of the relation $M = \hat{m}\sqrt{z_c z_d}$, the scale M is actually significantly lower than $\hat{m}$, typically by a factor 2. Our scale choices of M and $2M$ therefore roughly correspond to scales $\hat{m}/2$ and $\hat{m}$, and we refrain from using a scale lower than $\mu = M$ since this would correspond to a rather low scale at the partonic hard scattering.

Figure 1 shows the comparison to the NA24 [9] data for $pp \to \pi^0\pi^0 X$ at $\sqrt{S} = 23.7$ GeV. The cuts employed by NA24 are $|\cos\theta^*| < 0.4$, average over $|Y| < 0.35$, and $p_T^{\text{pair}} < 1$ GeV. We start by comparing the full NLO cross section to the first-order expansion of the resummed expression, that is, the last two terms in Eq. (48). This will help to gauge to what extent the soft-gluon terms constitute the dominant part of the cross section, so that their resummation is reliable. It turns out that the two terms agree to a remarkable degree. The dashed lines in Fig. 1 show the NLO cross section for scales $2M$ (lower) and M (upper), while the crosses give the NLO expansion of the resummed cross section. Their difference actually never exceeds 1% for the kinematics relevant for NA24. The solid lines and dash-dotted lines in the figure present the full, and matched, resummed results for the DSS and AKK fragmentation sets, respectively, including C coefficients implemented as described in Sec. III B [see Eq. (41)]. One can see that resummation leads to a very significant enhancement of the theoretical prediction. A very good description of the NA24 data [9] is obtained for both sets, much better than for the NLO calculation which falls short of the data unless rather low renormalization and factorization scales are used. Also the scale dependence of the calculated cross section is much reduced by resummation. We note that the resummed result for the AKK set shows a somewhat steeper M-dependence than that for the DSS set and lies lower at high M. This may in part be due to the fact that large-N resummation effects were included in the AKK analysis of the e^+e^- annihilation data, resulting probably in fragmentation functions that have an overall steeper z-dependence. That said, given the still relatively large uncertainties of fragmentation functions overall, we also note that the different behavior of the AKK and DSS results might be just due to differing assumptions made in the respective analyses.

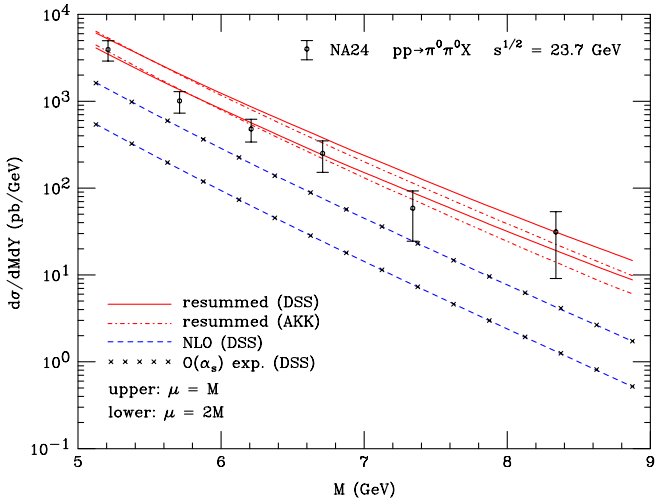

FIG. 1 (color online). Comparison of the NLO (dashed lines) and resummed [solid lines (DSS) and dash-dotted lines (AKK)] calculations to the NA24 data [9], for two different choices of the renormalization and factorization scales, $\mu = M$ (upper lines) and $\mu = 2M$ (lower lines). The crosses display the NLO $\mathcal{O}(\alpha_s)$ expansion of the resummed cross section.

We next turn to the cross section for charged-hadron production, $pBe \to h^{\pm}h^{\pm}X$, measured by E711 [10] at

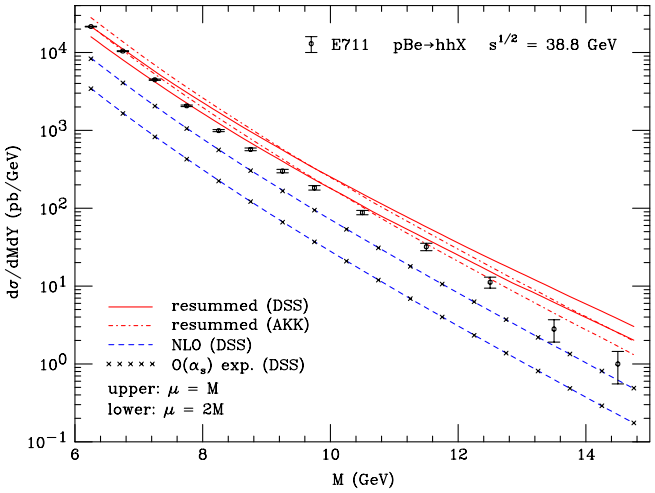

FIG. 2 (color online). Same as Fig. 1, but for charged-hadron production for pp scattering at $\sqrt{S} = 38.8$ GeV and with cuts appropriate for comparison to E711. The data are from [10].

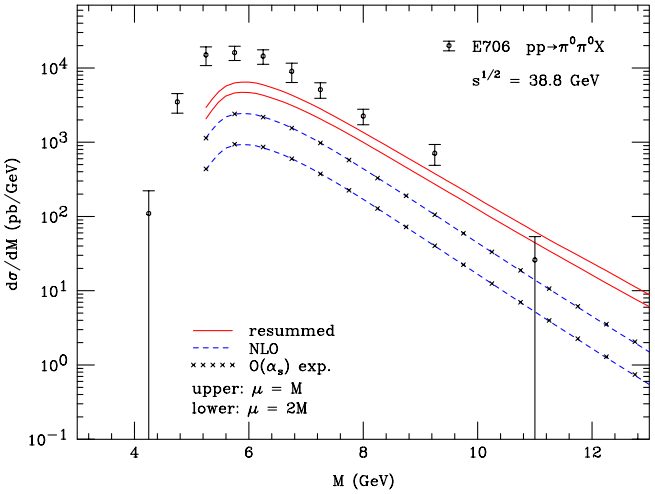

FIG. 3 (color online). Comparison of the NLO (dashed lines) and resummed (solid lines) calculations (for the DSS fragmentation set) to the E706 pp data at $\sqrt{S} = 38.8$ GeV [11], for two different choices of the renormalization and factorization scales, $\mu = M$ (upper lines) and $\mu = 2M$ (lower lines). The crosses display the NLO $\mathcal{O}(\alpha_s)$ expansion of the resummed cross section.

$\sqrt{S} = 38.8$ GeV. We recall that we sum over the charges of the produced hadrons. The cuts applied by E711 were $p_{T,i} > 2$ GeV, and average over $-0.4 < |Y| < 0.2$. The cut on the individual hadron transverse momenta is, in fact, irrelevant for the values of M considered here. Furthermore, as stated in Fig. 6 of [10] for the pair mass distribution we apply $p_T^{\text{pair}} < 2$ GeV, and $0.1 < |\cos\theta^*| < 0.25$. Figure 2 shows the data and our results. As before, the agreement between NLO and the NLO expansion of the resummed calculation is excellent. Again, resummation leads to an increase of the predicted cross section and a reduction of scale dependence. Even though the resummed results agree with the data much better than the NLO ones for the scales we have chosen, they tend to lie somewhat above the data, in particular at the highest values of M. Keeping in mind the results for NA24, one may wonder if this might be in part related to the fragmentation functions for summed charged hadrons, which are probably slightly less well understood than those for pions, due to the contributions from the heavier kaons and, in particular, baryons. The trend for the resummed result to lie a bit high is, however, somewhat less pronounced for the AKK set which again produces results that are a bit steeper than the DSS ones.

Figures 3 and 4 show the comparison of our results (for the DSS set) to the E706 data sets for neutral pion pair production in pp and pBe scattering at $\sqrt{S} = 38.8$ GeV (800 GeV beam energy), respectively. We do not take into account any nuclear effects for the beryllium nucleus, except for the trivial isospin one. This has a very minor effect on the cross section, compared to pp. E706 used cuts fairly different from those applied in the data we have discussed so far. There were no explicit cuts on $\cos\theta^*$, p_T^{pair} or Y, but instead cuts $p_{T,i} > p_T^{\text{cut}} = 2.5$ GeV and either $-1.05 < \eta_i < 0.55$ (for the $\sqrt{S} = 38.8$ GeV data) or $-0.8 < \eta_i < 0.8$ (for the $\sqrt{S} = 31.6$ GeV data) on the transverse momenta and rapidities of the individual pions. The cut on transverse momentum, in particular, has a strong influence at the lower M: in a rough approximation, it leads to a kinematic limit $M \sim 2p_{T,i} > 5$ GeV, so that the cross section has to decrease very rapidly once one decreases M toward 5 GeV. This behavior is indeed seen in the figures.

As in the previous cases, the NLO expansion of the resummed and the full NLO cross section agree extremely well, typically to better than 2%. For the two scales we have chosen, the NLO cross sections fall well short of the

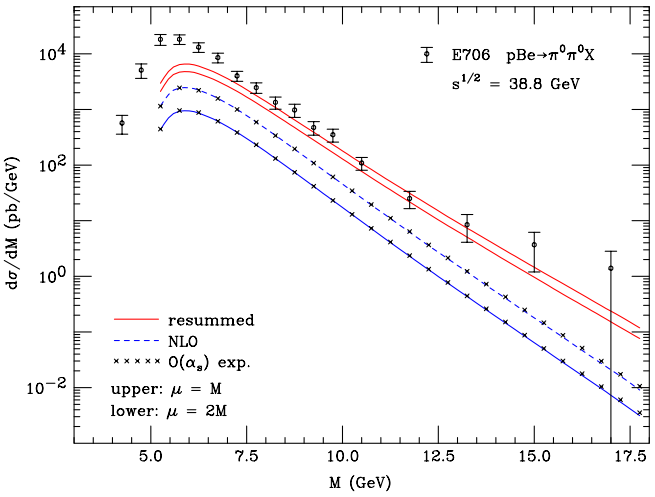

FIG. 4 (color online). Same as Fig. 3, but for proton-beryllium scattering.

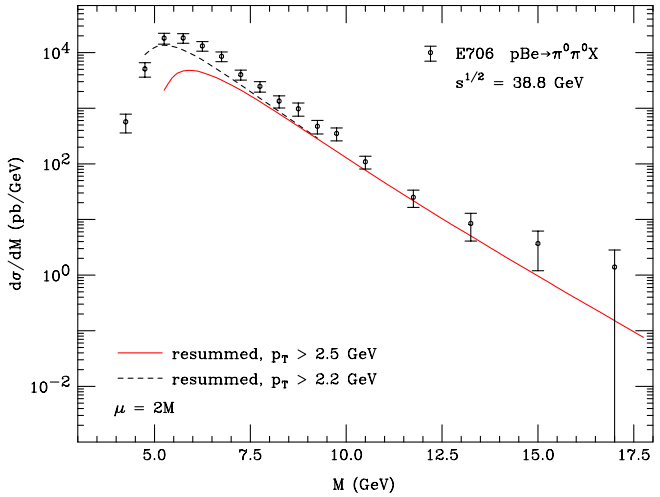

FIG. 5 (color online). Resummed cross section for scale $\mu = 2M$ and $p_{T,i} > 2.2$ GeV (dashed line), compared to the one with $p_{T,i} > 2.5$ GeV shown previously in Fig. 4 (solid line).

data. It was noted in [14,15] that in order for NLO to match the data, very low scales of $\mu = 0.35M$ have to be chosen. The resummed cross section, on the other hand, has much reduced scale dependence and describes the data very well for the more natural scales M and $2M$, except at the lower M where the cut $p_T^{\rm cut}$ on the $p_{T,i}$ becomes relevant. One observes that the data extend to lower M than the theoretical cross section, which basically cuts off at $M = 5$ GeV as discussed above. A new scale becomes relevant here, the difference $|M - 2p_T^{\rm cut}|$. Higher-order effects associated with this scale (which are different from the ones addressed by threshold resummation) and/or nonperturbative effects such as intrinsic transverse momenta [11] probably control the cross section here. It is also instructive to see that the cross section is very sensitive to the actual value of the cut

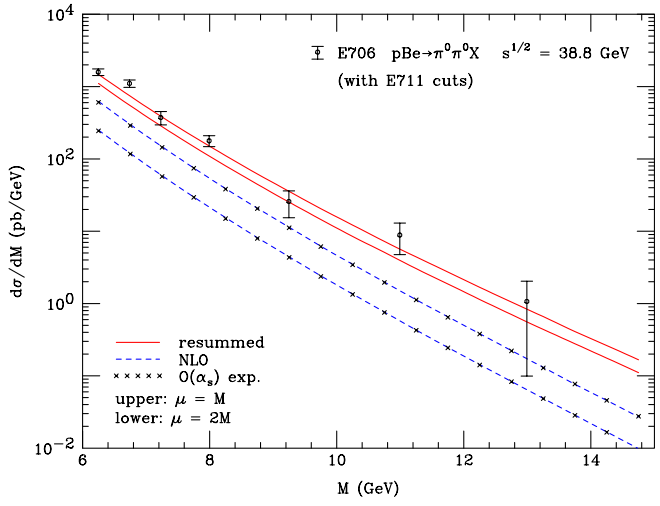

FIG. 6 (color online). Comparison to E706 data with a different set of cuts, corresponding to the ones applied by E711. The data with these cuts are from [11].

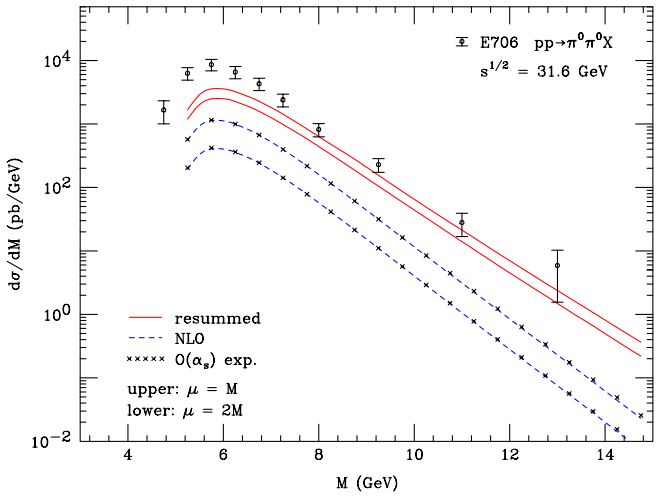

FIG. 7 (color online). Same as Fig. 3, but at $\sqrt{S} = 31.6$ GeV.

on the $p_{T,i}$. In Fig. 5 we show the resummed results for scale $\mu = 2M$ for $p_{T,i} > 2.5$ GeV (as before) and $p_{T,i} > 2.2$ GeV. One can see that with the lower cut the data are much better described. Experimental resolution effects might therefore have a significant influence on the comparison between data and theory here.

In order to check consistency, E706 also presented their pBe data set at $\sqrt{S} = 38.8$ GeV when the E711 cuts were applied instead of the E706 default ones. These data are found in [11]. Figure 6 shows the comparison for this case. One can see the same trends as before. Clearly, the description of the data by the resummed calculation is excellent. For this set of cuts, the cross section is not forced to turn down by kinematics at the lower M, and theory and data agree well everywhere. Figures 7 and 8 show results corresponding to Figs. 3 and 4, but for the lower beam energy, 530 GeV, employed by E706 ($\sqrt{S} = 31.6$ GeV).

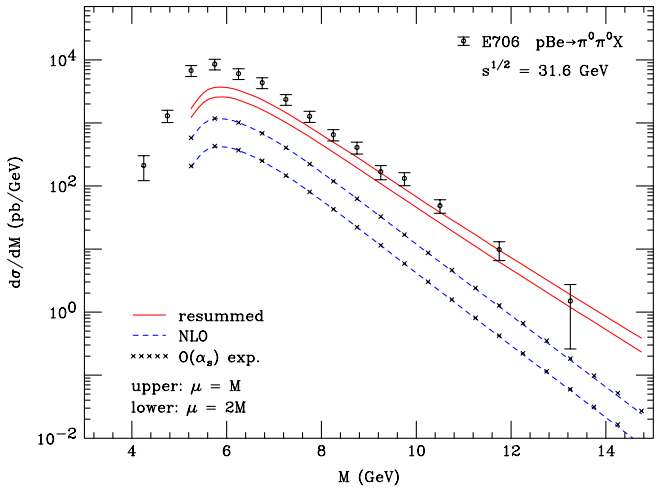

FIG. 8 (color online). Same as Fig. 4, but at $\sqrt{S} = 31.6$ GeV.

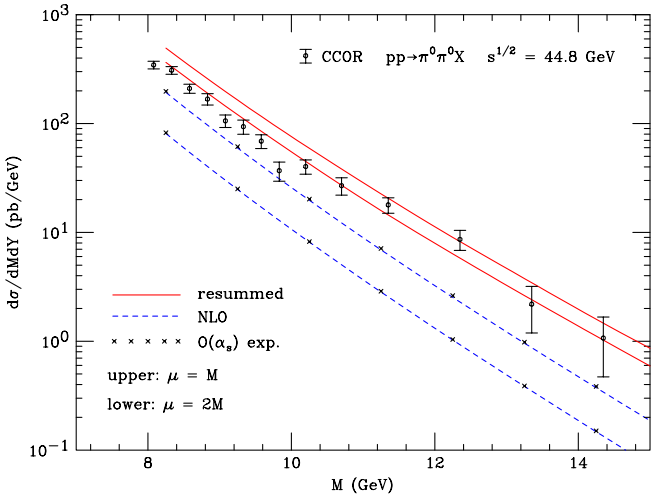

FIG. 9 (color online). Comparison of the NLO (dashed lines) and resummed (solid lines) calculations to the CCOR data [9] at $\sqrt{S} = 44.8$ GeV, for two different choices of the renormalization and factorization scales, $\mu = M$ (upper lines) and $\mu = 2M$ (lower lines). The crosses display the NLO $\mathcal{O}(\alpha_s)$ expansion of the resummed cross section.

We finally turn to the data sets available at the highest energy, which are from the CCOR experiment at the ISR [12]. Two data sets are available, at $\sqrt{S} = 44.8$ and 62.4 GeV. The cuts employed by CCOR were identical to those of NA24, $|\cos\theta^*| < 0.4$, average over $|Y| < 0.35$, and $p_T^{\text{pair}} < 1$ GeV. Figure 9 shows our results at $\sqrt{S} = 44.8$ GeV. The resummed calculation again shows decreased scale dependence and describes the data much better than the NLO one. At the lower values of M, it does show a tendency to lie above the data. Barring any issue with the data (which appear to have a certain unexpected "shoulder" around $M = 10$ GeV or so), this might indicate that one gets too far from threshold for resummation to be very precise. On the other hand, the agreement between full NLO and the NLO expansion of the resummed cross section still remains very good, as can be seen from the figure. The trend for resummation to give results higher than the data becomes more pronounced at the higher energy, $\sqrt{S} = 62.4$ GeV, as Fig. 10 shows, where we have used both the DSS and AKK sets of fragmentation functions. Although not easily seen from the figure, the NLO expansion of the resummed cross section starts to deviate more from the full NLO cross section than at the lower energies. At the lower M shown, it can be higher by up to 7%, which is still a relatively minor deviation, but could be indicative of the reason why the resummed result is high as well.

Clearly, any deviation between the full NLO cross section and the NLO expansion of the resummed one is due to terms that are formally suppressed by an inverse power of the Mellin moment N near threshold. It is therefore interesting to explore the likely effects of such terms. This can

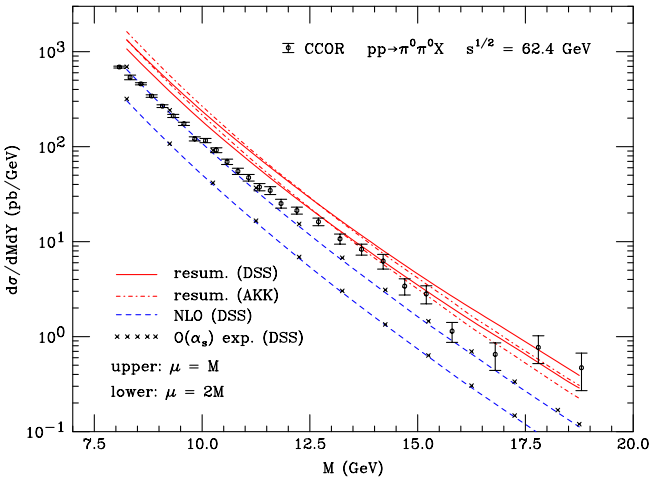

FIG. 10 (color online). Same as Fig. 9, but for $\sqrt{S} = 62.4$ GeV. We also show the resummed result obtained for the AKK set of fragmentation functions.

be done by promoting the LO anomalous dimension in the evolution part in Eq. (42) from its diagonal form to the full one, as described in Sec. III B:

$$-2A_i^{(1)} \ln\bar{N} - B_i^{(1)} \to P_{ij}^{(1),N}, \tag{52}$$

which includes the subleading terms in $1/N$ and full singlet mixing. For simplicity, we perform this modification only for the lowest order part of evolution, as indicated in Eqs. (43) and (52). The results obtained in this way are shown in Fig. 11. One can see that the resummed result obtained in this way indeed decreases significantly with respect to the one in Fig. 10 which was based on the diagonal evolution only, and is much closer to the data. At the same time, the agreement between the NLO cross

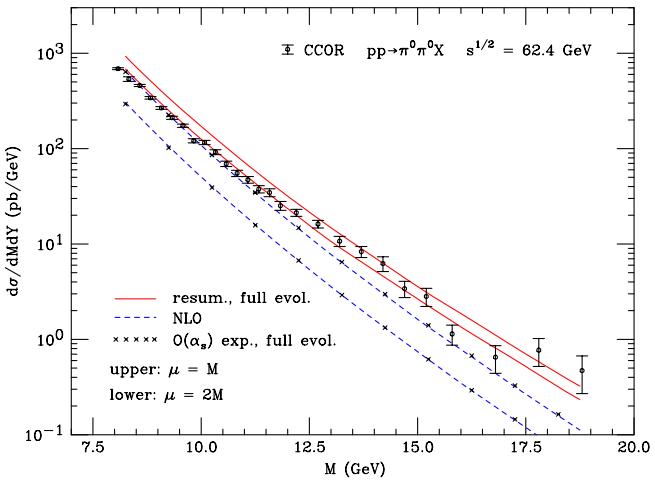

FIG. 11 (color online). As Fig. 10, but extending the diagonal evolution in the resummed formula to included subleading terms and singlet mixing, as shown in Eq. (52). We use the DSS set of fragmentation functions.

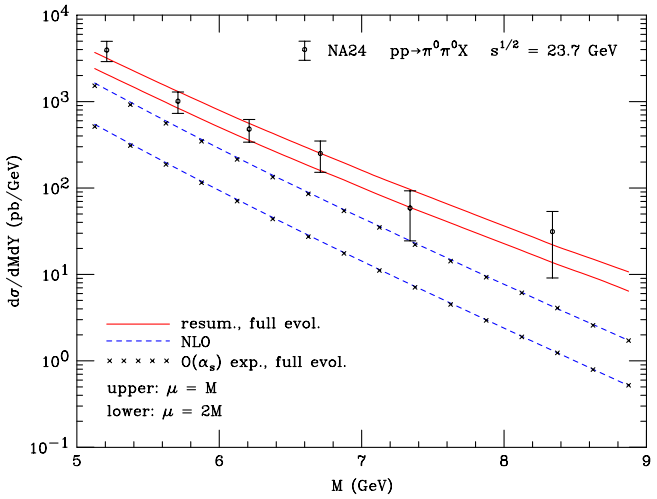

FIG. 12 (color online). Same as Fig. 11, but for the case of NA24.

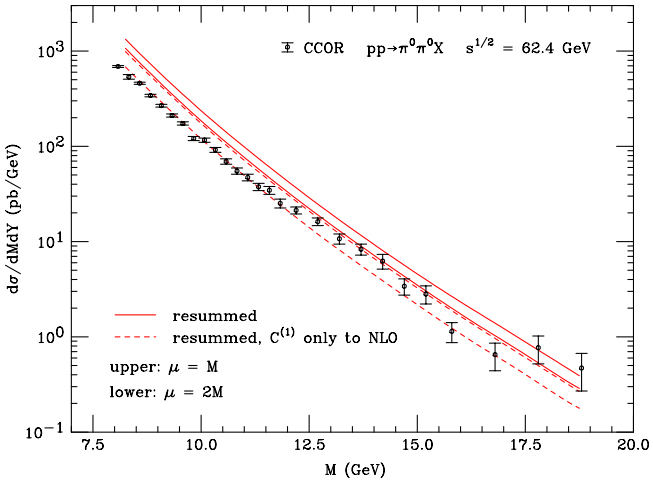

FIG. 13 (color online). Resummed results for the case of CCOR at $\sqrt{S} = 62.4$ GeV. The solid lines show the results for scales M and $2M$ shown previously in Fig. 10, while the dashed ones were obtained by neglecting the contributions by the $C^{(1)}_{ab\to cd}$ coefficients beyond NLO.

section and the $\mathcal{O}(\alpha_s)$ expanded resummed result becomes as good as what we encountered in the fixed-target case. Figure 12 presents the corresponding result for the case of NA24. Comparison with Fig. 1 shows that the effect of the subleading terms is much smaller here, as expected from the fact that one is closer to threshold in the case of NA24. Nonetheless, the effects lead to a slight further improvement between the resummed calculation and the data. In particular, they give the theoretical result a somewhat flatter behavior, which follows the trend of the data more closely overall. While the implementation of subleading terms in this way will require further study, this appears to be a promising approach for extending the applicability of threshold resummation into regimes where one is relatively far away from threshold.

That said, we remind the reader that already in the part that is leading near threshold we have made the approximation in Eq. (41) for our C coefficients. This, too, will need to be improved in the future, by taking into account the full color structure of the hard-scattering function beyond LO, as we discussed in Sec. III B. To give a somewhat extreme example of the effects generated by the C coefficients, we have recomputed the resummed cross section for the case of CCOR at $\sqrt{S} = 62.4$ GeV, but leaving out all effects of the coefficients *beyond NLO*. In other words, we leave out the C coefficients in the first two terms on the right-hand side of Eq. (48), keeping them of course in $d\sigma^{\rm NLO}$. This is likely not a good approximation of the beyond-NLO hard coefficients, because the $C^{(1)}_{ab\to cd}$ have π^2 terms and logarithms in the renormalization scale μ that are independent of the color channel and truly enter in the form given in Eq. (41). Some of these are in fact even known to exponentiate [17,20,21,31,40]. In any case, the result of this exercise is shown in Fig. 13, where it is also compared to our earlier calculation that included the C coefficients in the way discussed in Sec. III B. One can see that there is a sizable numerical difference, and that the scale dependence of the resummed result without the beyond-NLO C coefficients becomes significantly worse.

We finally turn to the distribution in $\cos\theta^*$, defined in Eq. (49), for which most of the experiments mentioned above have presented data as well. In fact, the CCOR data [12] for this observable were instrumental in establishing the QCD hard-scattering nature of pp interactions [41]. From the point of view of threshold resummation, the distribution in $\cos\theta^*$ may appear somewhat less interesting than the pair mass one, since the threshold logarithms arise in $1 - \hat{\tau} = 1 - \hat{m}^2/\hat{s}$, regardless of $\cos\theta^*$. In addition, the $\cos\theta^*$ distributions are presented as normalized distributions of the form

$$\frac{d\sigma/d\cos\theta^*}{d\sigma/d\cos\theta^*|_{\cos\theta^*=0}}, \tag{53}$$

so that the main enhancement generated by threshold resummation is expected to cancel. Nonetheless, as we have seen in Sec. III B, the resummed expressions do contain additional dependence on $\Delta\eta$ beyond that present in the Born cross sections, which will affect the $\cos\theta^*$ distribution at higher orders. This is visible from the soft part in Eq. (46) and also from the C coefficients in Eq. (41). Rather than going through an exhaustive comparison to all the available data, we just consider one example that is representative of the effects of threshold resummation on the $\cos\theta^*$ distribution. Figure 14 shows the normalized distribution for the E711 case, where we have again summed over all charge states of the produced hadrons. The dashed lines show the NLO result calculated again with the code of [14], for scales $\mu = 2M$ and $\mu = M$. One can see that for these scales the NLO calculation is lower

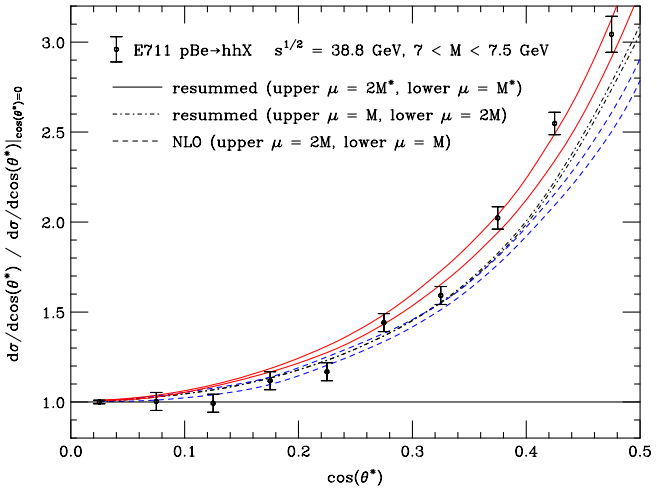

FIG. 14 (color online). Normalized distribution in $\cos\theta^*$ [see (53)] for the case of charged-hadron production at E711. Dashed line is NLO, while the dot-dashed lines and solid lines show resummed results. For the latter we have also used the scales $\mu = M^*$ and $\mu = 2M^*$, where $M^{*2} = M^2(1 - \cos\theta^*)$.

than the data for higher values of $\cos\theta^*$. The dot-dashed lines in Fig. 14 show the resummed results for scales $\mu = 2M$ and $\mu = M$. These show a steeper rise with $\cos\theta^*$ and describe the data better than NLO for the scales shown. However, they still tend to lie below the data at higher values of $\cos\theta^*$. As was suggested in [12,14,15], for the $\cos\theta^*$ distribution the hard scale in the partonic process will itself be a function of $\cos\theta^*$, so that it is more natural to choose a factorization/renormalization scale that reflects this feature. We therefore present our resummed results also for scales $\mu = 2M^*$ and $\mu = M^*$, where $M^{*2} = M^2(1 - \cos\theta^*)$ which is proportional to the Mandelstam variable $\hat{t}$ in the partonic process. One observes that with these scale choices a very good description of the data is achieved. We note that in the NLO calculations presented in Refs. [14,15] the scale was chosen proportional to the (average) transverse momenta of the produced hadrons, which for given M also depend on $\cos\theta^*$. This resulted in a satisfactory description of the data, when scales effectively a factor two smaller than our M^* were used. Overall, the trend for the resummed $\cos\theta^*$ distribution to lie higher than NLO and be in better agreement with the data is found to be a generic feature that occurs as well for the cases of the other experiments.

V. CONCLUSIONS

We have investigated the effects of next-to-leading logarithmic threshold resummation on the cross section for dihadron production in hadronic collisions, $H_1H_2 \to h_1h_2X$, for a range of invariant masses of the produced hadron pair. We have developed techniques to implement the resummation formalism at fixed rapidities for the produced hadrons and for all relevant experimental cuts. Extensions of these techniques to the level of next-to-next-to-leading logarithms should be relatively straightforward in light of the close relation between the one- and two-loop soft anomalous dimension matrices [42].

For the fixed-target and collider data studied here, the one-loop expansions of our resummed expressions approximate the corresponding exact one-loop cross sections excellently, to the level of a few percent and often less. In addition, with scales chosen to match the underlying hard scattering, the matched resummed cross sections typically explain the available data better than do NLO expressions at similar scales, with significantly reduced scale dependence.

An important extension of these methods will be in the production and fragmentation of heavy quarks and in jet cross sections, where similar resummation methods are applicable. Given the reduction in scale dependence, this could provide an improved control over standard model tests and backgrounds in new physics searches.

ACKNOWLEDGMENTS

We are grateful to M. Begel and H. B. White for very helpful communications on the E706 and E711 data, respectively, and to S. Albino, B. Jäger, A. Mitov, M. Stratmann and M. Tannenbaum for useful discussions. We also thank J. F. Owens for providing his NLO code for dihadron production, and for comments. W. V. is grateful to the U.S. Department of Energy (Contract No. DE-AC02-98CH10886) for providing the facilities essential for the completion of his work. This work was supported in part by the National Science Foundation, Grants No. PHY-0354776, No. PHY-0354822 and No. PHY-0653342.

APPENDIX A

In this appendix we present some details for the calculation of the NLO partonic cross sections near threshold. The virtual corrections have the $2 \to 2$ kinematics of the Born terms and therefore fully contribute. They are proportional to $\delta(1 - \hat{\tau})$. The real-emission $2 \to 3$ contributions require more effort. We consider the reaction $a(p_1) + b(p_2) \to c(k_1) + d(k_2) + e(k_3)$, where partons d and e fragment into the observed pair of hadrons and have pair mass $\hat{m}^2$. It is convenient to work in the c.m.s. of the observed outgoing hadrons. We can then write the three-body phase space in $4 - 2\varepsilon$ dimensions as

$$\Phi_3 = \frac{s}{(4\pi)^4\Gamma(1-2\varepsilon)}\left(\frac{4\pi}{s}\right)^{2\varepsilon}\int_0^1 d\hat{\tau}\hat{\tau}^{-\varepsilon}(1-\hat{\tau})^{1-2\varepsilon} \times \int_0^\infty d\rho\rho^{-\varepsilon}(1+\rho)^{-2+2\varepsilon}\int_0^\pi d\psi\sin^{1-2\varepsilon}\psi \times \int_0^\pi d\theta\sin^{-2\varepsilon}\theta. \tag{A1}$$

Here we define

$$\rho = (p_1 - k_2)^2/(p_2 - k_2)^2 = \mathrm{e}^{-2\Delta\eta}. \tag{A2}$$

Near threshold, the integration variables are given in terms of the Mandelstam variables of the process as follows:

$$\begin{aligned}
&(p_1 + p_2)^2 = \hat{s}, \qquad (k_2 + k_3)^2 = \hat{m}^2 = \hat{\tau}\,\hat{s},\\
&(p_1 - k_1)^2 = -\frac{\hat{s}(1-\hat{\tau})}{2}(1 - \cos\psi),\\
&(p_2 - k_1)^2 = -\frac{\hat{s}(1-\hat{\tau})}{2}(1 + \cos\psi),\\
&(p_1 - k_2)^2 = -\frac{\hat{s}\rho}{1+\rho} = (p_2 - k_3)^2,\\
&(p_2 - k_2)^2 = -\frac{\hat{s}}{1+\rho} = (p_1 - k_3)^2,\\
&(k_1 + k_2)^2 = \frac{\hat{s}(1-\hat{\tau})}{2}\left(1 + \sin\psi\cos\theta\,\frac{2\sqrt{\rho}}{1+\rho} - \cos\psi\,\frac{1-\rho}{1+\rho}\right),\\
&(k_1 + k_3)^2 = \frac{\hat{s}(1-\hat{\tau})}{2}\left(1 - \sin\psi\cos\theta\,\frac{2\sqrt{\rho}}{1+\rho} + \cos\psi\,\frac{1-\rho}{1+\rho}\right).
\end{aligned} \tag{A3}$$

The phase space in Eq. (A1) is used to integrate the squared $2 \to 3$ matrix elements $|\mathcal{M}_{ab\to cde}|^2$. For the latter one also assumes near-threshold kinematics. Since we want the partonic cross section at fixed $\hat{\tau}$ and $\Delta\eta$, we only need to perform the last two integrations in Eq. (A1). The basic integral for these is [43]

$$\begin{aligned}
&\int_0^\pi d\psi \int_0^\pi d\theta \frac{\sin^{1-2\varepsilon}\psi \sin^{-2\varepsilon}\theta}{(1-\cos\psi)^j(1-\cos\psi\cos\chi - \sin\psi\cos\theta\sin\chi)^k}\\
&= 2\pi\frac{\Gamma(1-2\varepsilon)}{\Gamma(1-\varepsilon)^2}2^{-j-k}B(1-\varepsilon-j, 1-\varepsilon-k)\,{}_2F_1\left(j, k, 1-\varepsilon, \cos^2\frac{\chi}{2}\right),
\end{aligned} \tag{A4}$$

where ${}_2F_1$ is the hypergeometric function. After integration over phase space and addition of the virtual corrections, infrared singularities cancel and only collinear singularities remain. These are removed by mass factorization, which we do in the $\overline{\mathrm{MS}}$ scheme. Notice that since we are close to threshold only the diagonal splitting functions $P_{ii}^{(1)}$ contribute in this procedure. Combining all contributions, one arrives at the near-threshold structure of the partonic cross sections given in Eq. (17), for each subprocess that is already present at LO. The final step is to take Mellin moments in $\hat{\tau}$ of the result, as described in Eq. (26). This gives for the partonic cross sections to NLO:

$$\begin{aligned}
&\tilde{\omega}_{ab\to cd}^{\mathrm{thr,LO+NLO}}(N, \Delta\eta, \alpha_s(\mu), \mu/\hat{m})\\
&= \omega_{ab\to cd}^{(0)}(\Delta\eta) + \frac{\alpha_s(\mu)}{\pi}\Big[\omega_{ab\to cd}^{(1,0)}(\Delta\eta, \mu/\hat{m})\\
&\quad - \ln\bar{N}\,\omega_{ab\to cd}^{(1,1)}(\Delta\eta, \mu/\hat{m}) + \frac{1}{2}(\ln^2\bar{N}\\
&\quad + \zeta(2))\omega_{ab\to cd}^{(1,2)}(\Delta\eta)\Big],
\end{aligned} \tag{A5}$$

where terms subleading in N have been neglected. The C coefficients defined in Eq. (41) are obtained from this as

$$\begin{aligned}
&C_{ab\to cd}^{(1)}(\Delta\eta, \mu/\hat{m})\\
&= \frac{\omega_{ab\to cd}^{(1,0)}(\Delta\eta, \mu/\hat{m}) + \frac{1}{2}\zeta(2)\omega_{ab\to cd}^{(1,2)}(\Delta\eta)}{\omega_{ab\to cd}^{(0)}(\Delta\eta)}.
\end{aligned} \tag{A6}$$

APPENDIX B

In this section we give the coefficients $C_{ab\to cd}^{(1)}$ for each subprocess contributing to the production of our dihadron final state, resulting from the calculation outlined in Appendix A. In all expressions below, μ is the renormalization scale. The dependence on the factorization scale is already included in the function $\mathcal{E}_i$ in Eq. (43). As before, we define $\rho \equiv \mathrm{e}^{-2\Delta\eta}$.

$qq' \to qq'$:

We define:

$$Q_{qq'} \equiv 1 + (1+\rho)^2. \tag{B1}$$

We then have:

$$C^{(1)}_{qq'\to qq'}(\Delta\eta,\mu/\hat{m}) = 2\pi b_0 \ln\frac{\mu^2}{\hat{m}^2} + \left(\frac{5}{6Q_{qq'}} + \frac{13}{12}\right)\ln^2\rho + \left(\frac{5}{6} - \frac{1}{3Q_{qq'}}\right)\ln^2(1+\rho) + \left(-\frac{8}{3} + \frac{14+9\rho}{6Q_{qq'}}\right)\ln\rho + \left(-\frac{4}{3} + \frac{2}{3Q_{qq'}}\right)\ln(1+\rho)\ln\rho - \frac{\rho}{3Q_{qq'}}\ln(1+\rho) + \frac{7\pi^2}{6Q_{qq'}} + \frac{N_f}{3}\ln\frac{\rho}{1+\rho} - \frac{5N_f}{9} + \frac{8}{3}\mathrm{Li}_2\left(\frac{\rho}{1+\rho}\right) + \frac{3}{2}\ln(1+\rho) + \frac{47\pi^2}{36} + \frac{7}{2}. \tag{B2}$$

$q\bar{q}' \to q\bar{q}'$:
We have:

$$C^{(1)}_{q\bar{q}'\to q\bar{q}'}(\Delta\eta,\mu/\hat{m}) = C^{(1)}_{qq'\to qq'}(\Delta\eta,\mu/\hat{m}) + \frac{5}{6}\left\{\left(1 - \frac{2}{Q_{qq'}}\right)\left[(1+\ln\rho)\ln\rho + \frac{\pi^2}{2}\right] - \frac{\rho}{Q_{qq'}}\ln(1+\rho) + \left(\frac{3}{2} - \frac{1}{Q_{qq'}}\right)\ln(1+\rho)\ln\frac{1+\rho}{\rho^2} - 2\mathrm{Li}_2\left(\frac{\rho}{1+\rho}\right)\right\}. \tag{B3}$$

$qq \to qq$:
We define:

$$Q_{qq} \equiv \frac{(1-\rho+\rho^2)(3+5\rho+3\rho^2)}{(1+\rho(1+\rho))}. \tag{B4}$$

We then have:

$$C^{(1)}_{qq\to qq}(\Delta\eta,\mu/\hat{m}) = 2\pi b_0 \ln\frac{\mu^2}{\hat{m}^2} + \frac{8}{Q_{qq}}(1-\rho^2)\mathrm{Li}_2\left(\frac{\rho}{1+\rho}\right) + \left(\frac{7}{6} - \frac{59\rho}{48Q_{qq}} + \frac{5}{4Q_{qq}} - \frac{\rho+4}{16(3+5\rho+3\rho^2)}\right)\ln^2\rho - \frac{(12\rho^2+3\rho-4)}{2Q_{qq}}\ln^2(1+\rho) + \frac{\ln\rho}{12Q_{qq}}\left(37\rho - 71 + \frac{(17-8\rho)Q_{qq}}{3+5\rho+3\rho^2}\right) + \left(\frac{7}{3} - \frac{7}{4Q_{qq}}(6-5\rho) - \frac{53\rho-6}{12(3+5\rho+3\rho^2)}\right)\ln(1+\rho)\ln\rho + \left(\frac{3}{2} - \frac{\rho}{4Q_{qq}} - \frac{\rho}{4(3+5\rho+3\rho^2)}\right) \times \ln(1+\rho) + N_f\left(\frac{2-\rho}{2Q_{qq}} + \frac{\rho}{3(3+5\rho+3\rho^2)}\right)\ln\rho - \frac{1}{3}N_f\ln(1+\rho) - \frac{5N_f}{9} + \frac{7}{2}\left(1 + \frac{2}{3}\pi^2\right) - \frac{\pi^2}{3Q_{qq}}\left(4 + \frac{41}{16}\rho\right) - \frac{71\pi^2\rho}{144(3+5\rho+3\rho^2)}. \tag{B5}$$

$q\bar{q} \to q'\bar{q}'$:
We define:

$$Q_{q'\bar{q}'} \equiv 1 + \rho^2. \tag{B6}$$

We then have:

$$C^{(1)}_{q\bar{q}\to q'\bar{q}'}(\Delta\eta,\mu/\hat{m}) = 2\pi b_0 \ln\frac{\mu^2}{\hat{m}^2} + \frac{7}{4}\left(1 - \frac{2}{3Q_{q'\bar{q}'}}\right)\ln^2\rho - \frac{5}{12}\left(1 + \frac{2}{Q_{q'\bar{q}'}}\right)\ln^2(1+\rho) + \frac{7(1+\rho)}{6Q_{q'\bar{q}'}}\ln\rho - \frac{7}{6}\left(1 - \frac{2}{Q_{q'\bar{q}'}}\right)\ln(1+\rho)\ln\rho - \frac{1}{3}\left(1 + \frac{5+9\rho}{2Q_{q'\bar{q}'}}\right)\ln(1+\rho) - \frac{5N_f}{9} - \frac{5}{3}\mathrm{Li}_2\left(\frac{\rho}{1+\rho}\right) + \frac{1}{6}(21+4\pi^2). \tag{B7}$$

$q\bar{q} \to q\bar{q}$:
We define:

$$Q^{(1)}_{q\bar{q}} \equiv 3 + \rho(1+\rho), \qquad Q^{(2)}_{q\bar{q}} \equiv 1 + 3\rho(1+\rho). \tag{B8}$$

We then have:

$$\begin{aligned} C^{(1)}_{q\bar{q}\to q\bar{q}}(\Delta\eta, \mu/\hat{m}) = {} & 2\pi b_0 \ln\frac{\mu^2}{\hat{m}^2} + N_f\left(\frac{1}{6} + (1+2\rho)\left(\frac{1}{8Q^{(1)}_{q\bar{q}}} + \frac{1}{8Q^{(2)}_{q\bar{q}}}\right)\right)\ln\left(\frac{\rho}{1+\rho}\right) + \mathrm{Li}_2\left(\frac{\rho}{1+\rho}\right)\left(\frac{5+4\rho}{2Q^{(1)}_{q\bar{q}}} + \frac{1+4\rho}{2Q^{(2)}_{q\bar{q}}} - \frac{1}{3}\right) \\ & + \pi^2\left(\frac{5(9+14\rho)}{96Q^{(1)}_{q\bar{q}}} + \frac{155+282\rho}{288Q^{(2)}_{q\bar{q}}} + \frac{43}{36}\right) + \left(\frac{4\rho-79}{64Q^{(1)}_{q\bar{q}}} + \frac{61+180\rho}{576Q^{(2)}_{q\bar{q}}} + \frac{65}{36}\right)\ln^2\rho \\ & + \left(\frac{13+124\rho}{64Q^{(1)}_{q\bar{q}}} + \frac{361+972\rho}{576Q^{(2)}_{q\bar{q}}} + \frac{29}{36}\right)\ln^2(1+\rho) + \left(\frac{7-\rho}{16Q^{(1)}_{q\bar{q}}} - \frac{35+71\rho}{48Q^{(2)}_{q\bar{q}}} - \frac{11}{12}\right)\ln\rho \\ & + \left(\frac{61-64\rho}{32Q^{(1)}_{q\bar{q}}} - \frac{247+576\rho}{288Q^{(2)}_{q\bar{q}}} - \frac{22}{9}\right)\ln(1+\rho)\ln\rho + \left(\frac{8+\rho}{16Q^{(1)}_{q\bar{q}}} + \frac{36+71\rho}{48Q^{(2)}_{q\bar{q}}} + \frac{7}{12}\right)\ln(1+\rho) \\ & - \frac{5N_f}{9} + \frac{7}{2}. \end{aligned} \tag{B9}$$

$q\bar{q} \to gg$:
We define:

$$G_{q\bar{q}} \equiv (1+\rho^2)(4-\rho+4\rho^2). \tag{B10}$$

We then have:

$$\begin{aligned} C^{(1)}_{q\bar{q}\to gg}(\Delta\eta, \mu/\hat{m}) = {} & 2\pi b_0 \ln\frac{\mu^2}{\hat{m}^2} - \frac{27}{2G_{q\bar{q}}}(1-\rho^4)\mathrm{Li}_2\left(\frac{\rho}{1+\rho}\right) + \frac{1}{48}\left(1 + \frac{2\rho}{G_{q\bar{q}}}(133+13\rho) + \frac{124-311\rho}{4-\rho+4\rho^2}\right)\ln^2\rho \\ & + \frac{1}{48}\left(69 + \frac{52\rho^2}{G_{q\bar{q}}} - \frac{\rho+648}{4-\rho+4\rho^2}\right)\ln^2(1+\rho) + \frac{1}{6}\left(-\frac{\rho}{G_{q\bar{q}}}(3+89\rho) + \frac{48+5\rho}{4-\rho+4\rho^2}\right)\ln\rho \\ & + \left(\frac{89\rho^2}{3G_{q\bar{q}}} - \frac{19\rho}{6(4-\rho+4\rho^2)} - 2\right)\ln(1+\rho) + \frac{1}{24}\left(-19 - \frac{2\rho}{G_{q\bar{q}}}(133+13\rho) + \frac{200+149\rho}{4-\rho+4\rho^2}\right) \\ & \times \ln\rho\ln(1+\rho) - \frac{15}{4G_{q\bar{q}}}\rho(1-\rho)^2 + \frac{9\pi^2(4-\rho)}{16(4-\rho+4\rho^2)} + \frac{191\pi^2}{144} - \frac{14}{3}. \end{aligned} \tag{B11}$$

$qg \to qg$:
We define:

$$Q^{(1)}_{qg} \equiv 2(1+\rho) + \rho^2, \qquad Q^{(2)}_{qg} \equiv 9(1+\rho) + 4\rho^2. \tag{B12}$$

We then have:

$$\begin{aligned} C^{(1)}_{qg\to qg}(\Delta\eta, \mu/\hat{m}) = {} & 2\pi b_0 \ln\frac{\mu^2}{\hat{m}^2} - \frac{14}{3} + \frac{15(1+\rho)(2+\rho)^2}{4Q^{(1)}_{qg}Q^{(2)}_{qg}} + \pi^2\left(\frac{146+13\rho}{24Q^{(1)}_{qg}} - \frac{3(109+13\rho)}{16Q^{(2)}_{qg}} + \frac{241}{144}\right) \\ & + \left((1+\rho)\left(\frac{13}{12Q^{(1)}_{qg}} - \frac{15}{16Q^{(2)}_{qg}}\right) + \frac{17}{16}\right)\ln^2\rho + (1+\rho)\left(\frac{89}{3Q^{(1)}_{qg}} - \frac{231}{2Q^{(2)}_{qg}}\right)\ln\rho \\ & + \left(\frac{13\rho-120}{24Q^{(1)}_{qg}} + \frac{3(173+41\rho)}{16Q^{(2)}_{qg}} - \frac{27}{16}\right)\ln^2(1+\rho) + \left(-\frac{86+89\rho}{6Q^{(1)}_{qg}} + \frac{3(43+39\rho)}{2Q^{(2)}_{qg}} - 2\right)\ln(1+\rho) \\ & + \left(\frac{31}{24} + \frac{27(\rho-3)}{8Q^{(2)}_{qg}}\right)\mathrm{Li}_2\left(\frac{\rho}{1+\rho}\right) + \left(\frac{120-13\rho}{12Q^{(1)}_{qg}} - \frac{3(155+23\rho)}{8Q^{(2)}_{qg}} + \frac{31}{24}\right)\ln\rho\ln(1+\rho). \end{aligned} \tag{B13}$$

$gg \to q\bar{q}$:
We have:

$$C^{(1)}_{gg\to q\bar{q}}(\Delta\eta, \mu/\hat{m}) = C^{(1)}_{q\bar{q}\to gg}(\Delta\eta, \mu/\hat{m}). \tag{B14}$$

$gg \to gg$:
We define:

$$G_{gg} \equiv 1 + \rho(1+\rho). \tag{B15}$$

We then have:

$$\begin{aligned}
C^{(1)}_{gg\to gg}(\Delta\eta, \mu/\hat{m}) = {} & 2\pi b_0 \ln\frac{\mu^2}{\hat{m}^2} + N_f\left(\frac{5}{9} + \frac{3\rho^2(1+\rho)^2}{8G^3_{gg}} + \frac{\pi^2\rho(1+\rho^2)(1+\rho)^2}{16G^3_{gg}}\right) - \frac{3\rho^2(1+\rho)^2}{8G^3_{gg}}(3+\pi^2) \\
& + \frac{3}{4}\left(\frac{(1+\rho)^3}{G^3_{gg}} + 1\right)\ln^2\rho + \frac{N_f}{16G^2_{gg}}(1+\rho)\left(\frac{2}{G_{gg}}(1+\rho)^2 + \rho^2 - 2(1+\rho)\right)\ln^2\rho \\
& + \frac{N_f}{24G^2_{gg}}(8(1+\rho^2)+5\rho)(1+\rho)^2\ln(1+\rho) - \frac{N_f}{24G^2_{gg}}(1+\rho)(5\rho^2+8(1+\rho))\ln\rho \\
& + \frac{N_f}{16G^2_{gg}}(1+\rho)^2\left(\frac{2}{G_{gg}}(1+\rho) - 2 - \rho\right)\ln^2(1+\rho) + \frac{N_f}{8G^2_{gg}}(1+\rho)\left(2\rho + 1 - \frac{1}{G_{gg}}(1+\rho)^2\right) \\
& \times \ln\rho\ln(1+\rho) + \frac{1}{G^2_{gg}}\left(-\frac{11}{2}(1+\rho^2) - \frac{7}{4}\rho\right)(1+\rho)^2\ln(1+\rho) \\
& + \frac{1}{G^2_{gg}}\left(\frac{7}{4}\rho^2 + \frac{11}{2}(1+\rho)\right)(1+\rho)\ln\rho + \frac{3\pi^2(1+\rho)}{4G^2_{gg}} + \left(\frac{3}{2} - \frac{3(1+\rho)^3}{4G^3_{gg}} + \frac{3(2\rho+1)(1+\rho^2)}{4G^2_{gg}}\right) \\
& \times \ln\rho\ln(1+\rho) + \left(\frac{3(1+\rho)^3}{4G^3_{gg}} - \frac{3(2\rho+1)}{4G^2_{gg}} - \frac{3(1+\rho)}{2G_{gg}} - \frac{3}{4}\right)\ln^2(1+\rho) \\
& - \frac{3}{2G_{gg}}(1-\rho^2)\mathrm{Li}_2\left(\frac{\rho}{1+\rho}\right) - \frac{\pi^2(1+\rho)}{2G_{gg}} + \frac{11\pi^2}{4} - \frac{67}{6}.
\end{aligned} \tag{B16}$$

[1] P. Aurenche, M. Fontannaz, J. P. Guillet, B. A. Kniehl, and M. Werlen, Eur. Phys. J. C **13**, 347 (2000).
[2] U. Baur *et al.*, arXiv:hep-ph/0005226.
[3] C. Bourrely and J. Soffer, Eur. Phys. J. C **36**, 371 (2004).
[4] B. A. Kniehl, G. Kramer, and B. Pötter, Nucl. Phys. **B597**, 337 (2001).
[5] D. de Florian and W. Vogelsang, Phys. Rev. D **71**, 114004 (2005).
[6] A. Adare *et al.* (PHENIX Collaboration), Phys. Rev. D **76**, 051106 (2007); **79**, 012003 (2009).
[7] J. Adams *et al.* (STAR Collaboration), Phys. Rev. Lett. **97**, 152302 (2006).
[8] I. Arsene *et al.* (BRAHMS Collaboration), Phys. Rev. Lett. **98**, 252001 (2007).
[9] C. De Marzo *et al.* (NA24 Collaboration), Phys. Rev. D **42**, 748 (1990).
[10] H. B. White *et al.* (E711 Collaboration), Phys. Rev. D **48**, 3996 (1993); H. B. White, Ph.D. thesis, Florida State University (FERMILAB-THESIS-1991-39, FSU-HEP-910722, UMI-92-02321, 1991).
[11] M. Begel (E706 Collaboration), Ph.D. thesis, Rochester University (FERMILAB-THESIS-1999-05, UMI-99-60725, 1999); see also: L. Apanasevich *et al.* (E706 Collaboration), Phys. Rev. Lett. **81**, 2642 (1998).
[12] A. L. S. Angelis *et al.* (CCOR Collaboration), Nucl. Phys. **B209**, 284 (1982).
[13] P. Chiappetta, R. Fergani, and J. P. Guillet, Z. Phys. C **69**, 443 (1996).
[14] J. F. Owens, Phys. Rev. D **65**, 034011 (2002).
[15] T. Binoth, J. P. Guillet, E. Pilon, and M. Werlen, Eur. Phys. J. C **24**, 245 (2002); Eur. Phys. J. direct C **4**, 1 (2002).
[16] G. Sterman, Nucl. Phys. **B281**, 310 (1987); S. Catani and L. Trentadue, Nucl. Phys. **B327**, 323 (1989); **B353**, 183 (1991).
[17] N. Kidonakis and G. Sterman, Nucl. Phys. **B505**, 321 (1997).

[18] R. Bonciani, S. Catani, M. L. Mangano, and P. Nason, Phys. Lett. B **575**, 268 (2003).
[19] A. Idilbi, X. d. Ji, and F. Yuan, Nucl. Phys. **B753**, 42 (2006); T. Becher, M. Neubert, and G. Xu, J. High Energy Phys. 07 (2008) 030.
[20] N. Kidonakis, G. Oderda, and G. Sterman, Nucl. Phys. **B525**, 299 (1998); **B531**, 365 (1998).
[21] N. Kidonakis and J. F. Owens, Phys. Rev. D **63**, 054019 (2001).
[22] E. Laenen and G. Sterman, in *The Fermilab Meeting, DPF 1992* (World Scientific, Singapore, 1993), Vol. 1, p. 987.
[23] G. Sterman and W. Vogelsang, J. High Energy Phys. 02 (2001) 016.
[24] A. Mukherjee and W. Vogelsang, Phys. Rev. D **73**, 074005 (2006).
[25] G. Bozzi, S. Catani, D. de Florian, and M. Grazzini, Nucl. Phys. **B791**, 1 (2008).
[26] G. Sterman and W. Vogelsang, Phys. Rev. D **74**, 114002 (2006).
[27] M. Cacciari and S. Catani, Nucl. Phys. **B617**, 253 (2001).
[28] J. Kodaira and L. Trentadue, Phys. Lett. B **112**, 66 (1982); **123**, 335 (1983); S. Catani, E. D'Emilio, and L. Trentadue, Phys. Lett. B **211**, 335 (1988).
[29] L. G. Almeida, G. Sterman, and W. Vogelsang, Phys. Rev. D **78**, 014008 (2008).
[30] M. Sjodahl, J. High Energy Phys. 09 (2009) 087.
[31] N. Kidonakis, E. Laenen, S. Moch, and R. Vogt, Phys. Rev. D **64**, 114001 (2001).
[32] For related studies in heavy flavor production, see: R. Bonciani, S. Catani, M. L. Mangano, and P. Nason, Nucl. Phys. **B529**, 424 (1998); **B803**, 234 (2008); S. Moch and P. Uwer, Phys. Rev. D **78**, 034003 (2008); M. Czakon and A. Mitov, Phys. Lett. B **680**, 154 (2009).
[33] A. Kulesza, G. Sterman, and W. Vogelsang, Phys. Rev. D **66**, 014011 (2002).
[34] S. Catani, D. de Florian, and M. Grazzini, J. High Energy Phys. 05 (2001) 025; see also: M. Krämer, E. Laenen, and M. Spira, Nucl. Phys. **B511**, 523 (1998); R. V. Harlander and W. B. Kilgore, Phys. Rev. D **64**, 013015 (2001).
[35] S. Catani, M. L. Mangano, P. Nason, and L. Trentadue, Nucl. Phys. **B478**, 273 (1996).
[36] W. K. Tung, H. L. Lai, A. Belyaev, J. Pumplin, D. Stump, and C. P. Yuan, J. High Energy Phys. 02 (2007) 053.
[37] D. de Florian, R. Sassot, and M. Stratmann, Phys. Rev. D **75**, 114010 (2007).
[38] S. Albino, B. A. Kniehl, and G. Kramer, Nucl. Phys. **B803**, 42 (2008).
[39] H. Shimizu, G. Sterman, W. Vogelsang, and H. Yokoya, Phys. Rev. D **71**, 114007 (2005).
[40] T. O. Eynck, E. Laenen, and L. Magnea, J. High Energy Phys. 06 (2003) 057; E. Laenen and L. Magnea, Phys. Lett. B **632**, 270 (2006); E. Laenen, G. Stavenga, and C. D. White, J. High Energy Phys. 03 (2009) 054; E. Laenen, L. Magnea, and G. Stavenga, Phys. Lett. B **669**, 173 (2008).
[41] M. J. Tannenbaum, Nucl. Phys. **A749**, 219 (2005).
[42] S. M. Aybat, L. J. Dixon, and G. Sterman, Phys. Rev. D **74**, 074004 (2006); Phys. Rev. Lett. **97**, 072001 (2006); E. Gardi and L. Magnea, J. High Energy Phys. 03 (2009) 079; T. Becher and M. Neubert, J. High Energy Phys. 06 (2009) 081.
[43] W. L. van Neerven, Nucl. Phys. **B268**, 453 (1986).